Scientific Research Publishing

World Journal of Engineering and Technology, 2022, 10, 363-409
https://www.scirp.org/journal/wjet
ISSN Online: 2331-4249
ISSN Print: 2331-4222

Aspects of the Powder in Metal Additive Manufacturing: A Review

Gladius Lewis

Department of Mechanical Engineering, The University of Memphis, Memphis, USA
Email: glewis@memphis.edu

How to cite this paper: Lewis, G. (2022) Aspects of the Powder in Metal Additive Manufacturing: A Review. *World Journal of Engineering and Technology*, **10**, 363-409.
https://doi.org/10.4236/wjet.2022.102022

Received: February 20, 2022
Accepted: May 22, 2022
Published: May 25, 2022

Abstract

The most widely used metal additive manufacturing processes utilize powder that is spread or fed onto a building platform. Although there are reviews of the literature on some aspects of the powder, many aspects have been under-reviewed or unreviewed. The present work is a review of the literature on these aspects. Articles published in the open literature through the end of February 2022 were collected by consulting highly regarded relevant bibliographic databases, such as Google Scholar and Science Direct. The aspects reviewed were emerging methods of powder production, methods used to improve the quality of a powder after production by a well-established method, influence of variables of well-established powder production methods on powder properties, influence of powder production method on powder properties, and influence of powder reuse on properties of powders of a wide collection of alloys. One key finding was that with regard to powder reuse, the only consistent finding is that it leads to increase in the oxygen content of the powder. Another key finding was that the literature on the aspects of the literature reviewed herein contains many shortcomings and gaps, which suggest potential areas for future research, such as techniques for optimization of process variables for a given combination of metal powder and powder production method and development of methods for production of powders of new/emerging metallic materials.

Keywords

Metal Powder Feedstock, Metal Additive Manufacturing, Particle Size Distribution, Morphology, Flowability, Rheological Properties of Metal Powder

1. Introduction

The list of metal additive manufacturing (MAM) processes/technologies is very

long, with one basis for their categorization being the form of the starting raw material (Figure 1). It is worth noting that the MAM processes space is dynamic, with frequent introduction of novel processes, such as fused filament fabrication and hot-wire arc AM [1] [2] [3] [4]. Currently, powder-on-bed fusion processes are the most widely used, notably, laser beam powder bed fusion (LB-PBF) methods such as DMLS/SLS, SLM, and electron beam powder bed fusion (EB-PBF) [5]-[16]. The advantages, shortcomings, and challenges of MAM, compared to subtractive processes, such as casting, forging, and extrusion, are well documented [7] [8] [10] [11] [12] [14] [17]-[25]. Advantages include high degree of customization and minimal waste of raw/starting materials (for example, buy-to-fly ratios for a typical subtractive manufacturing method and MAM are ~20 and ~1, respectively). Among the shortcomings of MAM are high surface roughness (which results in poor dimensional accuracy of the built part), high incidence of near-surface and/or surface-connected porosity, and limited knowledge of the process-properties-performance relationship. Challenges facing MAM include a limited number of metallic materials that have been printed using this technique and limited certification of parts for some industries (notably the aerospace industry). The consensus is that the overarching attraction of MAM is that it can be used to fabricate parts with complex geometry [14] and, as such, over the years, it has been used to manufacture a growing list of components and structures for use in myriad industrial sectors and non-industrial fields [14].

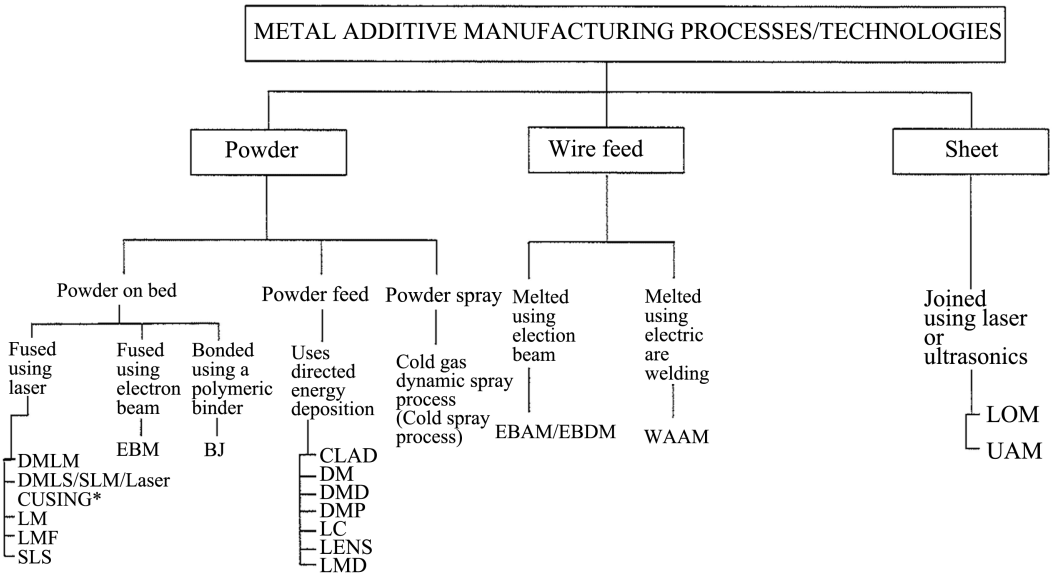

Figure 1. Categorization of metal additive manufacturing processes/technologies. DMLM: direct metal laser melting; DMLS: direct metal laser sintering; SLM: sintered laser melting; LM: laser melting; LMF: laser metal fusion; SLS: selective laser sintering; EBM: electron beam melting; BJ: binder jetting; CLAD: construction laser additive directed; DM: direct manufacturing; DMD: direct metal deposition; DMP: direct metal printing; LC: laser consolidation; LENS: laser-engineered net-shaping; LMD: laser metal deposition; EBAM: electron beam additive manufacturing; EBDM: electron beam direct melting; WAAM: wire and arc additive manufacturing; LOM: laminated object manufacturing; UAM: ultrasonic additive manufacturing.

In powder-based MAM methods, the importance of the powder feedstock is underscored by the fact that its cost (typically, unit cost is in the range of $40 - 500/kg) is a large proportion of the total normalized manufacturing cost of a part (defined as the sum of raw material, printing, and post-processing costs per volume of built part); for example, for both LB-PBF and EB-PBF, powder cost is ~40% [9] [23]. An additional indication of the importance of the powder is that its properties exert a marked influence on both the build rate of the part (and, hence, the production cost of the part) and its properties, especially its densification mechanism (and, hence, its porosity and mechanical properties) [9] [26] [27] [28] [29] [30].

There is a sizeable body of literature on many aspects of the powder feedstock used in MAM, and there are a number of reviews of this body but, with the exception of two reviews, their focus has been on three aspects. These are descriptions of and comments on advantages and shortcomings of established powder production methods (**Figure 2**) [11] [31]-[41]; powder characterization methods [27] [30] [42]; and the influence of powder properties on properties of built parts [26] [27] [29] [30] [41] [43] [44]. One of the exception reviews covered an overview of powder-bed MAM methods, powder flowability, raking behavior/powder layer formation, and brief discussion of the influence of powder properties and powder reuse on properties of both the powder and the built parts [29]. In the other exception review, in addition to covering established powder production methods, the issue of powder reusability/recycling vis-à-vis properties of powders of Ti, Ni, and Al alloys was addressed, and some of the coverage was on the influence of powder reuse on properties of built parts [41].

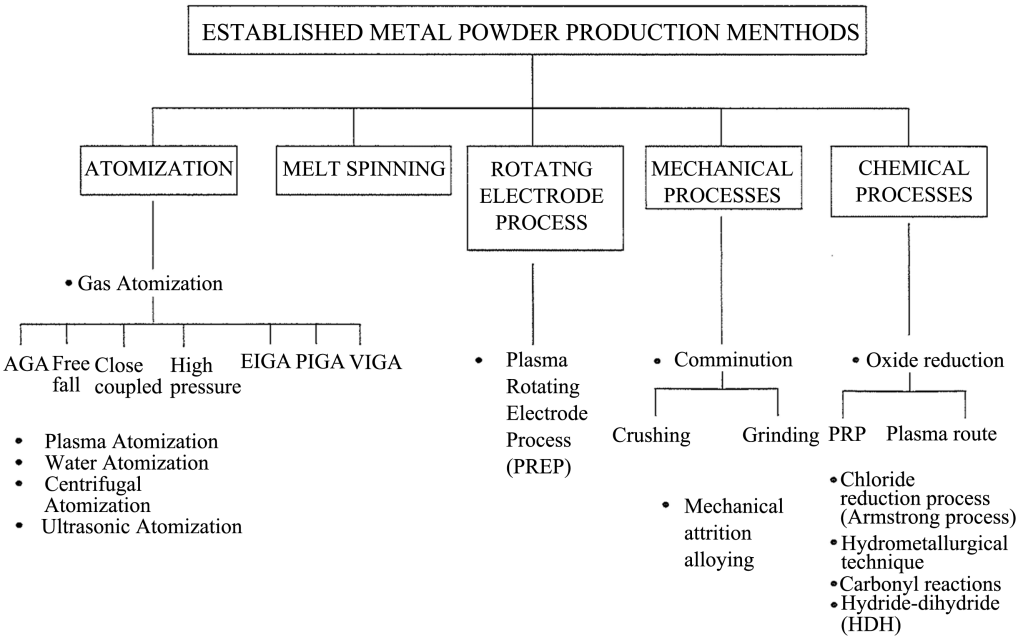

Figure 2. Categorization of well-established metal powder production methods. AGA: advanced gas atomization; EIGA: electrode induction melting gas atomization; PIGA: plasma melting inert gas atomization; VIGA: vacuum induction inert gas/argon atomization; PRP: preform reduction process.

The present review is focused exclusively on the powder feedstock, with its purpose being to present a comprehensive, detailed, and critical review of a large number of hitherto neglected aspects of the literature on powder and its properties. To that end, the review is divided into 7 parts, with one each devoted to features (principles, process variables, advantages, and shortcomings) of emerging powder production methods; post-production methods for treating powders produced using an established method; influence of process variables, for a given established powder production method, on powder properties; influence of established powder production method on powder properties; influence of powder reuse on properties of powder produced using established methods; an appraisal of the literature; and a summary of the main points made in the review.

2. Emerging Powder Production Methods

There are many emerging methods, with a suggested typology of them being shown in **Figure 3**. Salient aspects of nine of these methods are now given.

2.1. Plasma and Gas Hybrid Atomization (PGHA)

The first step in the development of the PGHA system [45] (**Figure 4(a)**) was optimization of the design of the anode (nozzle) for a direct current arc plasma torch (DCAPT). The constraints on the geometry, size, gas flow rate, and input power range of the DCAPT were that the length of the anode must be <0.55 m so that it is compatible with standard specifications of commercially-available GA systems. Operational conditions for the DCAPT were power, pressure of the nitrogen gas supplied to the gas injection ports, and nitrogen gas flow rate = 15 - 20 kW, 1.5 MPa, and 80 standard liters/min, respectively, yielding a thermal efficiency of ~80%. In running the system, three DCAPTs were used to ensure that

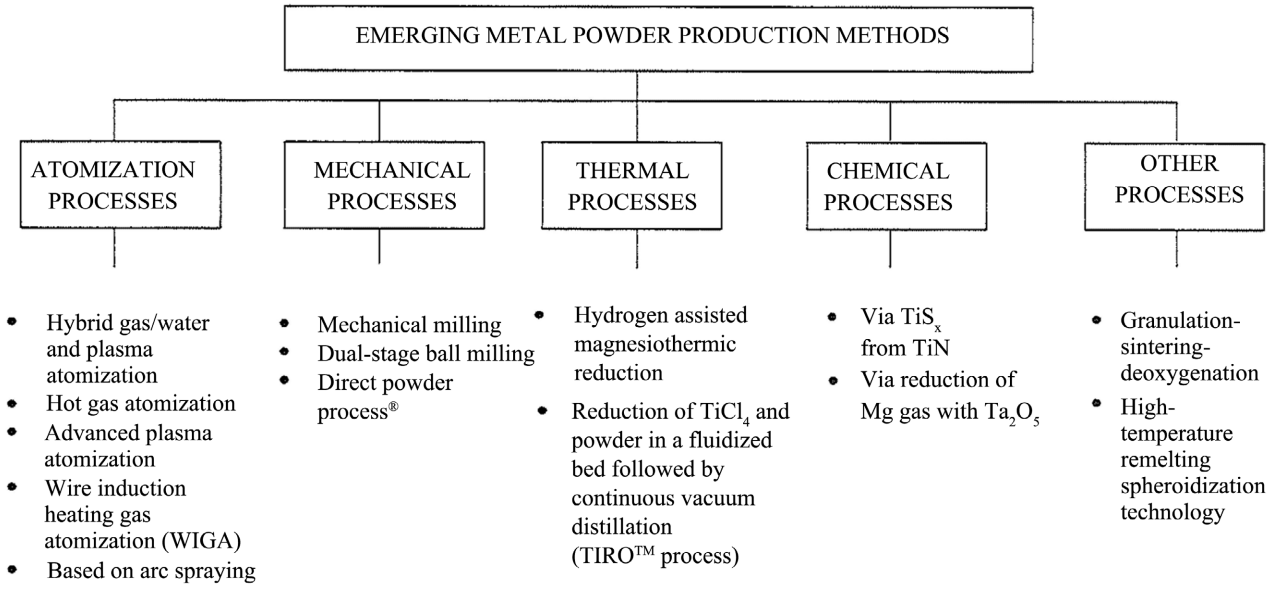

Figure 3. Categorization of emerging metal powder production methods.

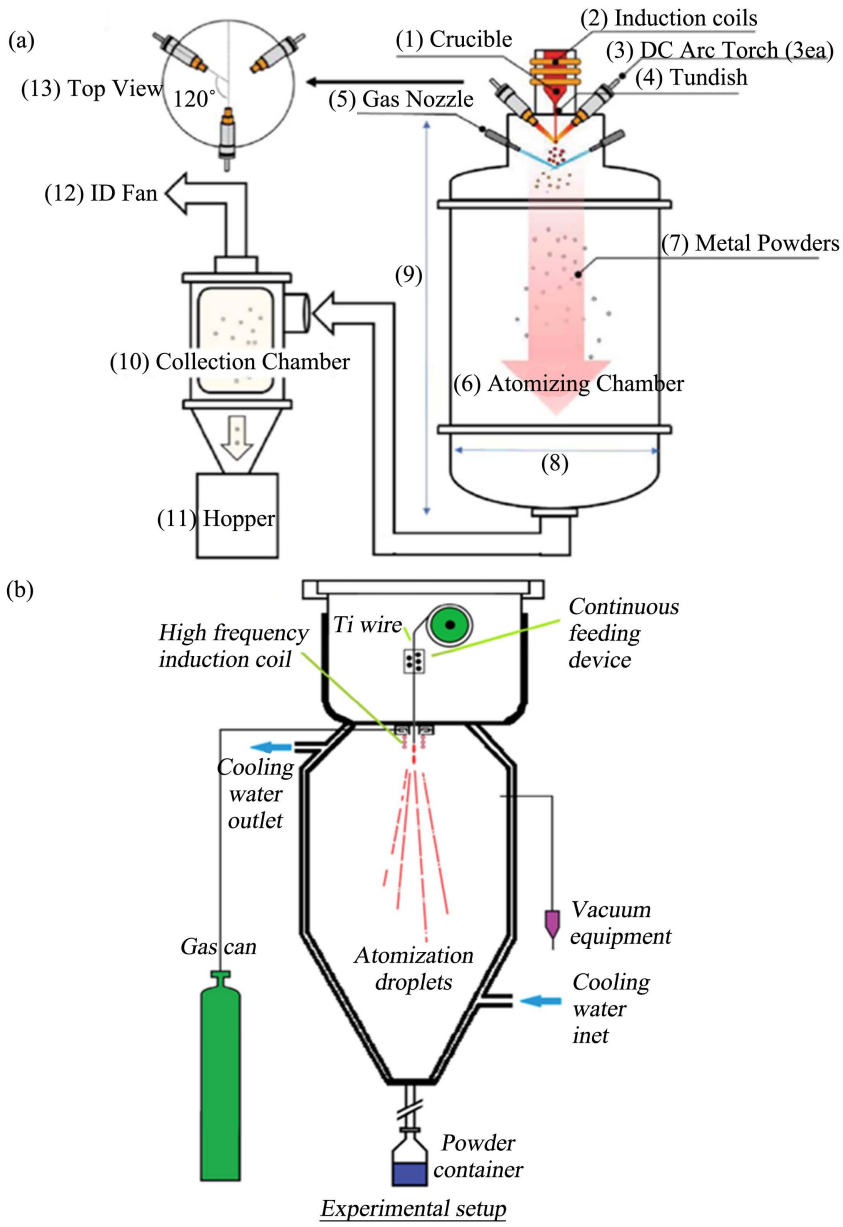

Figure 4. Schematic drawings of the plasma and gas hybrid plasma atomization (PGHA) system (a) [45] and the wire induction heating gas atomization (WIGA) set-up (b) [46].

the molten metal coming through a tundish was wetted in the plasma jet, thereby guaranteeing that atomization was achieved. Using the aforementioned operational conditions, spherical Sn powders (mean particle diameter (D_m) < 10 μm)), Cu powders (D_m < 50 μm), and stainless steel powders (D_m < 10 μm) were produced. Three important process variables of the PGHA system are the composition of the injection gases, the hole diameter of the tundish at the crucible, and the pressure of gas injection.

2.2. Wire Induction Heating Gas Atomization (WIGA)

The essence of the WIGA process [46] (**Figure 4(b)**) is the combination of

high-frequency induction melting of a metal wire and gas atomization technology, with Ar gas being used as both the atomizing gas (pressure = P_1) and the auxiliary shielding gas (pressure = P_2). Use of a crucible-less melting method ensured that the Ti melt was not contaminated during the melting process.

Three important process variables of the WIGA system are the wire feed speed (V_f), P_1, and the superheating temperature of the metal melt (T_s). In the case of Ti powder, median particle diameter (D_{50}) increased with increase in V_f, decreased with increase in P_2, and decreased with increase in T_s. Using the optimum values of these variables and P_2 = 3 MPa, the Ti powder obtained was spherical and smooth, with the following properties: D_{50} = 40.2 μm, oxygen gas (O) content = 0.12 wt./wt%, tap density (ρ_{tap}) = 2.81 g/cm^3, bulk density (ρ_{bulk}) = 2.52 g/cm^3, and flowability = 30 s/50g.

2.3. Arc Spraying

Arc spraying is a wire-based process in which the heat of an arc is transferred directly into the material [34]. An important process variable is the atomization medium (compressed air or Ar gas). With compressed air, there were chemical reactions with molten particles and formation of an oxide layer. This layer formed very quickly on the droplet surface and the surface tension of the molten material was not high enough for spherical particles to form. With Ar gas, the powder particles were more spherical and markedly smoother (compared to particles produced using compressed air), and the microstructure was highly refined (comprising a fine dispersed silicon phase at the grain boundaries).

2.4. Mechanical Milling

There are a few studies in which waste from a subtractive manufacturing process, namely, machining, was converted to powder that may be suitable for use in MAM [47] [48].

Segmented-type chips of an Al alloy (AA7075) were produced during machining of a rod billet in a lathe [47]. Then, the chips were processed in a double roller crusher, after which the chips were milled using a high-energy planetary ball mill in tungsten carbide vials that had been sealed and purged with high-purity Ar gas prior to the ball milling process. Milling time (t_m) ranged from 0.5 h to 10 h. Milling took place in an Ar gas atmosphere, at 400 rpm. To prevent excessive cold welding of the particles during the milling, a methanol solution was used as a process control agent. A ball milling model was presented, according to which ball-chip-ball collisions dominated when t_m was ≤5 h, while ball-powder-ball collisions dominated when t_m > 5 h. Particle diameter decreased monotonically with increase in t_m.

In another study, serrated 304L stainless steel chips (length: 5 - 20 mm) were used [48]. A model, which was a combination of Gusten's model and Hertz's model, was used to show that when balls with diameter (D_b) = 20 mm were used for the milling, the size of the particles in the final powder was reduced whereas

when balls with D_b = 6 mm were used, the morphology of the particles was changed, to spherical or near-spherical particles. These findings provided the rationale for using a dual-stage ball milling method, which yielded particles that were spherical or near-spherical (particle diameter (D) = 38 – 150 μm).

2.5. Hydrogen Assisted Magnesiothermic Reduction (HAMR)

HAMR involves four steps, namely, reduction, granulation, sintering, and deoxygenation [49].

At each of these stages, the morphology of the product had distinctive features. After reduction, the morphology did not change significantly and ~95% of O gas was removed; the granulated powder was spherical; and the individual powder particles sintered very well, with only a very small amount of adhesion taking place. The final powder was 100% dense and its O, C, and N contents were each lower than the levels given in the relevant materials standard specification (ASTM B299 [50]).

2.6. Continuous Process, TiRO™

There are two steps in the continuous process (TiRO™), as was used for the production of commercially-pure Ti powder [51] [52]. The first step was conducted in a fluidized bed, where $TiCl_4$ gas and Mg powder reacted to form small-sized Ti particles (D = ~1.5 μm). The reaction mechanism involved deposition of reaction products around the Mg particles. At the end of this step, some of the Ti particles contained small amounts of unreacted Mg as well as some internal voids. The second step involved vacuum distillation, in which $MgCl_2$ particles (produced in the first step) were removed from the Ti particles. The vacuum-distilled Ti formed a lightly sintered "biscuit", the majority of which easily broke loose from the belt at the discharge end. This "biscuit" was very lightly ground to yield spheroidal particles (D_m = ~200 μm). With further grinding, an angular Ti powder was produced. The final particle properties were influenced by grinding rate. For example, when the vacuum-distilled product was ground very vigorously (using a ring grinder), the O content of the final powder was very high, suggesting that this method of grinding may not be appropriate.

2.7. Variant of Ono and Suzuki Process

With this process, the production of Ti metal powder from $FeTiO_3$ involved nitridation (via TiN), sulfurization (via TiS_x), and the Ono and Suzuku (ONSU) process [53]. The starting material was TiN. $Ti_{2.45}S_4$ and TiS_2 powders were formed from TiN at 1200˚C in 3.6 and 10.8 ks, respectively. For the sulfurization process, S_2 or CS_2 gas may be used. When S_2 gas was used, the sulfur powder was evaporated in a dual-zone furnace, at a low temperature (typically, ~300˚C). S_2 gas was transferred into the hot zone of the reactor, from where a high-purity Ar gas (≥99.9998%) stream moved it to the reaction site. The sulfides obtained in the first step were converted to a-Ti metal powders by an electrochemical reduc-

tion (ONSU process) in a molten $CaCl_2$-CaS salt. The final α-Ti powder had spherical morphology and foil-like Ti sheets and an O content of <0.15 wt./wt%.

2.8. Granulation-Sintering-Deoxygenation (GSD)

There are four steps in the GSD process [54] (**Figure 5(a)**). The first involved ball milling the raw material (200 mesh Ti-6Al-4V hydride powder) in a mixture of a solvent and a thermoplastic binder (which aids formulation of granules), for, typically, 100 min, thereby reducing D to <10 μm. In the second step, the resulting slurry obtained at the end of the first step was fed into a spray dryer and dried with Ar gas, forming spherical granules that consisted of fine Ti-6Al-4V

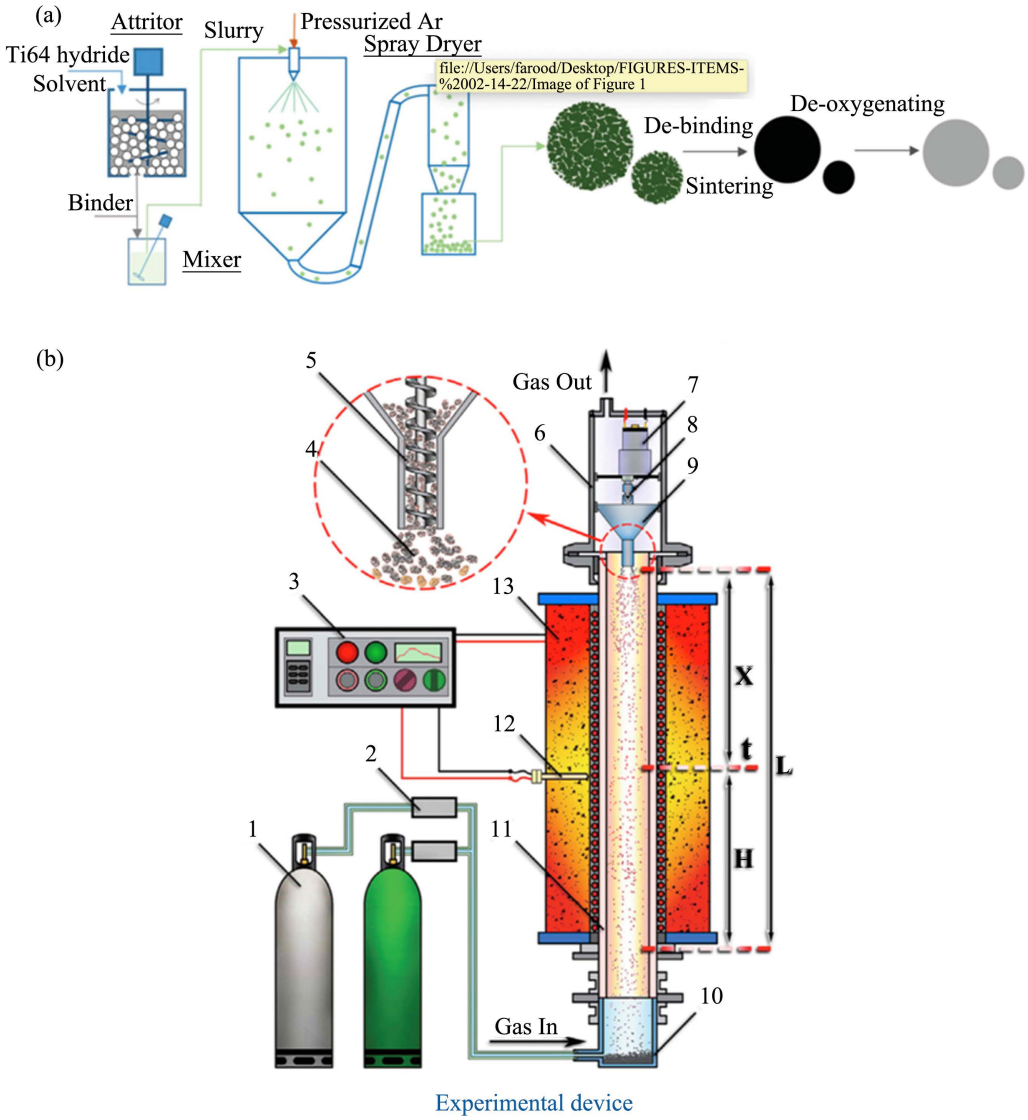

Figure 5. Flowchart of the steps involved in production of Ti-6Al-4V alloy powder from scrap using the granulation-sintering-deoxygenation (GSD) method (a) [54]; and a schematic drawing of the high-temperature remelting spheroidization (HTRS) process (b): 1: gas cylinder; 2: gas flowmeter; 3: thermal controller; 4: powder; 5: screw; 6: powder holder; 7: electric motor; 8: cardan joint; 9: feeding hopper; 10: collection tube; 11: corundum tube; 12: thermocouple; 13: electric furnace [55].

hydride particles. During Steps 1 and 2, an inorganic separator (CaO powder) was used to prevent adhesion of granules. In the third step, the granules were thermally debinded and, then, sintered in an Ar gas atmosphere in a tube furnace. After sintering, the CaO powder was leached with dilute HCl, washed with water and, then, dried in air at room temperature. In the fourth step, a low-temperature molten salt process was used to deoxygenate the spherical sintered powder.

Some properties of the final Ti-6Al-4V powder obtained using the process variable values stated above are: bulk O content = 0.10 ± 0.01 wt./wt%; fully densified particles that have a fine lamellar microstructure; D: 20 – 90 μm; apparent density (ρ_{app}) = 2.34 ± 0.02 g/cm^3; tap density (ρ_{tap}) =2.78 ± 0.02 g/cm^3; true density (ρ_{true}) = 99.5% ± 0.1%); and flowability = 27.5 ± 0.3 s/50g.

2.9. High-Temperature Remelting Spheroidization (HTRS) [55]

In the HTRS process (**Figure 5(b)**), which takes place in a reducing atmosphere (75 vol./vol% argon and 25% vol./vol. hydrogen), the feedstock was placed in a hopper and then fed into a furnace tube by a screw feeder, after which the powder was dispersed in the air evenly. When the powder passed through the high-temperature zone in the furnace, the in-flight metal particles were rapidly heated and melted into liquid drops, which, due to surface tension, produced spherical particles. When HRTS was used to produce Cu particles, the process variables that influenced the values/range of values of particle size were: temperature (1100˚C - 1350˚C), particle feed rate (0.1013 - 0.3920 g/min), and sheath gas flow rate (150 or 50 mL/min when Ar gas or hydrogen gas was used, respectively).

Six aspects of the process were presented in detail, these being particle behavior in flight, settling process, heat transfer process, spheroidization, influence of feed rate, and influence of ambient temperature. Very brief summaries of these aspects, when Cu powder was produced, are now given.

For particle behavior in flight, Stokes formula was used to calculate the falling time and the instant velocity of Cu powder. After that, the temperature of the particles was obtained by combining the conservation energy equation with the heat transfer equation. For the settling process, three simplifications were used. First, since D was in the range of 45 - 125 μm, the Brownian force and the thermophoresis force were neglected. Second, since the density of the Cu powder >> than that of the gas, the buoyancy, additional mass force, and Basset force were considered negligible. Third, the particles were considered subject only to hydrodynamic resistance. The required settling time and D were found to be inversely related; for example, the settling times of 125 μm- and 45 mm-sized particles were 0.95 s and 5.55 s, respectively. The calculation of heat exchange was based on two assumptions. First, heat conduction inside the particle was considered fast because D is small; as such, the temperature distribution in the interior of the particle was assumed to be uniform and the particle shape was taken to be spherical. Second, the powder was taken to comprise fine particles that

were scattered evenly at an appropriate feed rate. Particles were regarded as a sparse phase compared to the gas phase. A heat balance equation was developed, which presented the relationship between particle temperature (T_p) and environment temperature, from which T_p was obtained and found to vary with displacement. It was found that the residence time of the particles in the high-temperature region of the furnace is an important variable.

At 1350˚C, Cu spherical powder, with smooth surfaces and no satellite particles, homogeneous in microstructure, and fully dense with no pores, was obtained. For this powder, there was marked decrease in O content, marked increase in bulk density, and marked increase of flowability of HTRS-treated variant compared to corresponding values for the initial powder.

At a given particle feedstock feed rate (FR), HTRS treatment led to a narrowing of the particle size distribution (PSD) of the final powder. However, when FR was very high, the particles agglomerated. Also, at very high FR, the powder adhered to the furnace tube wall and, when sufficient build-up occurred, it fell off in large chunks, resulting in a significant reduction of the spheroidization rate (defined as the ratio of volume of spherical particles to that of non-spherical particles).

With increase in ambient temperature (T_{amb}), the O content of the HTRS-treated powder increased very slightly while the spheroidization rate of the powder increased markedly. Most of the 45 - 125 μm-sized particles spheroidized at T_{amb} = 1300˚C, and, at T_{amb} = 1350˚C, all the particles were perfectly spherical, with bright smooth surfaces. As such, it was suggested that it may not be necessary to use T_{amb} > 1300˚C.

3. Post-Production Modification Methods

One variable investigated was the method of preparation of Ti-6Al-4V alloy powder feedstock through a process known as "*in situ* alloying of elemental powder mixtures" [56]. The four study groups in this study were 1) commercially-available powder produced using gas atomization (GA) ("pre-alloyed powder" group); 2) simple mixing of the elemental powders purchased from vendors: Ti powders sieved to obtain particle sizes in the range of 45 – 75 μm, Al powder sieved at 45 μm, and V powders with PSD of D_{10}, D_{50}, and D_{90} = 6.39, 21.2, and 45.8 μm, respectively ("simply mixed powder 1" group); 3) simple mixing of the Ti powder used in group 2 with fine Al powder (D_{10}, D_{50}, and D_{90} = 2.8, 6.2, and 12.2 μm, respectively) and V powder (D_{10}, D_{50}, and D_{90} = 6.39, 21.2, and 45.8 μm), respectively) ("simply mixed powder 2" group); and 4) the Ti, Al, and V powders were mixed using a method called "satellite mixing", which has three steps. First, the Ti powder, the fine Al powder and the V powder were dry mixed to yield a homogeneous mixture. Second, this mixture was mixed with a polyvinyl alcohol (PVA) solution until the liquid was fully dispersed through the mixture, after which the mixture was mixed in an agitator. Third, the mixture was dried in an oven and then passed through a 75-μm sieve. The morphology and flowability of each of the four powders were determined.

With regard to morphology, the particles in the pre-alloyed powder were uniformly spherical; in simply-mixed 1 powder, there were regions where Ti or Al aggregated; in the simply-mixed powder 2, random Ti particles were decorated by Al clusters; in the satellite-mixed powder, there were zones with high Al and V contents (a consequence of the presence of some large-sized V particles) and varying amounts of satellites on the Ti particles because of the irregular particle size and morphology of the particles and insufficient wetting of the powder mixture by the PVA. The difference in the morphologies of the four powders is reflected in their flowabilities (**Table 1**), which show that preparation of a feedstock by mixing the constituent element powders may not improve its processability for use in a powder-based MAM process.

Two key components of the inductively-coupled plasma process (ICPP) (a plasma spheroidization process developed by a commercially entity, Tekna Plasma Systems, Inc.) are an inductively coupled plasma torch placed on top of a water-cooled stainless steel chamber [57] (**Figure 6(a)**). In the process, a carrier/diluent gas and a water-cooled injection probe were used to inject the powder into the center of the discharge. As the individual powder particles were heated

Table 1. Influence of process variables on a selection of powder properties.

Powder[a]	Mean particle size (μm)	Oxygen content (%)	Oxide layer thickness (nm)	Flowability (s/50g)	ρ_{app} (g/cm^3)	ρ_{tap} (g/cm^3)	Ref.
Ti-6Al-4V powder							Simonelli *et al.* [56]
As-received (PA)				32.4 ± 0.5			
Simply mixed 1							
Simply mixed 2				40.0 ± 1.0			
Satellite-mixed				36.12 ± 0.07			
Ti-6Al-4V powder							Vert *et al.* [57]
As-received (HDH)	90 - 340	3017 ppm		50	1.89	2.32	
After ICP[b] treatment	70 - 200	2100 ppm		23	2.74	2.95	
Ti powder							Ding *et al.* [60]
As-received (HDH)	28.6	0.35	6				
FBR[b] treatment, at 450˚C	30.5	0.39	10	35.2 ± 0.3			
FBR treatment, at 500˚C	32.5	0.50		32.6 ± 0.2			
FBR treatment, at 550˚C	33.9	0.80		40.0			
FBR treatment, at 600˚C	31.8	1.50	20	73.5 ± 0.5			

[a]Method of production of as-received powder; PA: plasma atomization; HDH: hydride-dihydride. [b]ICP: inductively-coupled plasma spheroidization process; FBR: fluidized bed reactor, with treatment time = 10 min.

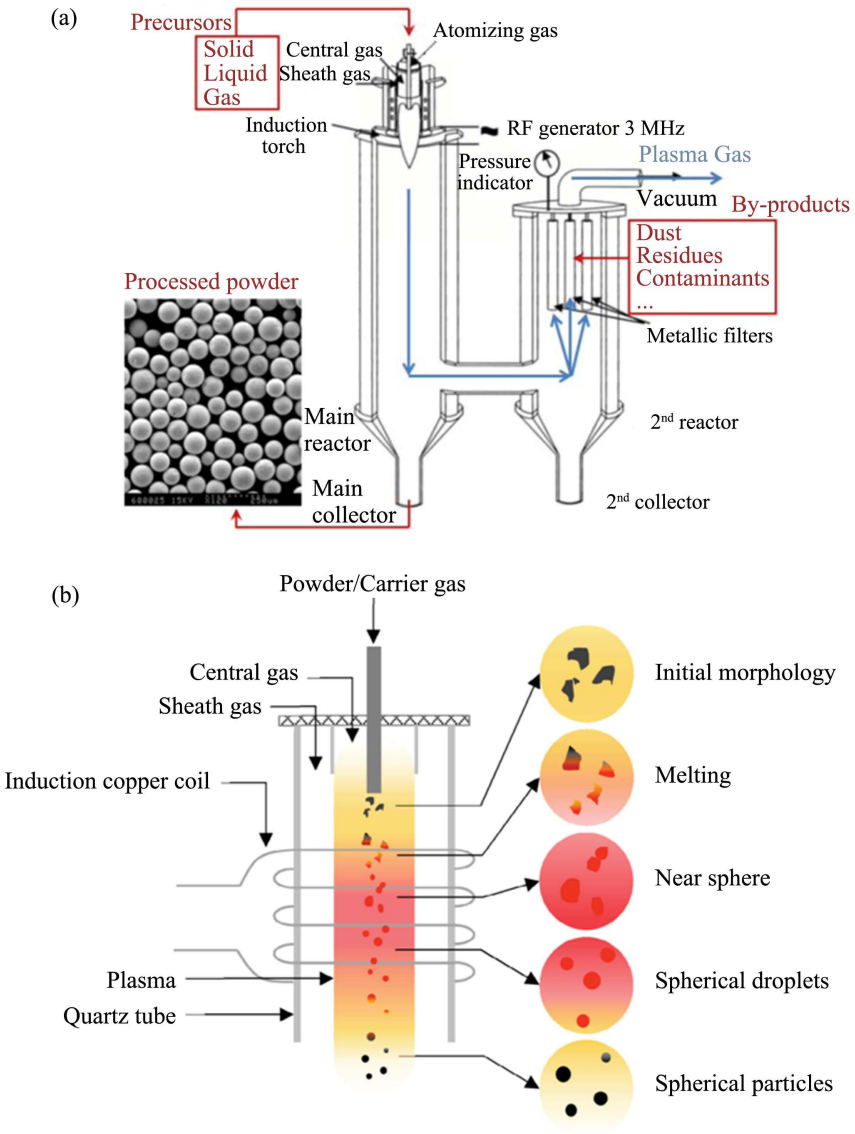

Figure 6. Schematic drawings of Tekna's powder spheroidization process (a) [57] and the radiofrequency inductively coupled plasma spheroidization process (b) [59].

and melted in the plasma, they formed spherical dense molten metal droplets, which cooled and solidified as they dropped to the bottom of the chamber. The processed powders were recovered at the bottom of the chamber, while the plasma gases and any vapors or ultrafine powders exited through a side port and were directed to a sintered metal filter, from where the gases were sent to the vacuum pumping and exhaust system. The ICPP system may be operated over a wide range of plasma gas mixtures at atmosphere pressure or soft vacuum. The plasma can be used as a chemical reactor as well as an enthalpy source, which means that the system may be used to spheroidize a starting powder regardless of its method of production. The ICPP has been used to treat commercially-pure Ti powder [57], Grade 23 Ti-6Al-4V alloy powder [57], and Zr-4 alloy powder [58].

Properties of Grade 23 Ti-6Al-4V powder produced using the hydride-dehydride (HDH) method and, then, treated using ICPP, have been compared [57]. On the ICPP-treated powder, in addition to powder spheroidization, there were "satellites", which was attributed to the partial vaporization of the particles during its plasma heating and melting, followed by the condensation of the formed vapors on the surface of the particles in the cooling phase of their trajectory, resulting in soft deposits on the surface of the larger particles. When these deposits were removed, a high-quality powder was obtained (**Table 1**) [57].

Irregular-shaped Zr-4 alloy powder particles with rough edges and sharp corners, produced using HDH, were transformed to spherical ones using ICPP, accompanied by marked drops in the O and hydrogen gas contents of the powder (~35% and ~90%, respectively) (attributed to absorption of oxygen, high degree of oxidation, and further dehydrogenation at elevated temperature during ICCP) and marked narrowing of the PSD (D_{10}, D_{50}, and D_{90} of HDH-produced and ICPP-treated HDH-produced powders were 1.011, 7.129, and 65.631 μm, and 44.057, 60.464, and 82.744 μm, respectively) [58]. In terms of phase composition, HDH-produced powder consisted of α-Zr and residual hydrides (ZrH and $ZrH_{1.66}$) formed during the HDH process, whereas after ICPP treatment, the powder consisted of α-Zr phase only [58].

A variant of ICCP, namely, a radio frequency inductively-coupled plasma system [59] (**Figure 6(b)**) was used to transform irregularly-shaped Ta powders to spherical ones that were contaminated with oxygen and contained a small number of irregular-shaped particles. Compared to the starting powder, the PSD of the spheroidized powder was narrower (D_{50} for the starting and spheroidized powders were ~60 and ~55 μm, respectively) and possessed ~27% higher ρ_{app}, ~17% higher ρ_{tap}, and ~36% higher flowability.

The influence of treating Ti powder produced using HDH, in a high-temperature fluidizing process, on the morphology, PSD, flowability, and O content of the powder was investigated [60]. The powder was treated in a fluidized bed reactor (FBR), under high-purity Ar gas, flowing at a steady rate and a temperature (T_{bed}) that varied between 450˚C and 600˚C, for 10 min ("FBR powder"). The as-received powder particles were irregularly shaped and had sharp edges whereas, in the FBR powder, the particles had smoother edges (attributed to the drag force that occurred during the treatment) and some particles with $D < 5$ μm were either partially embedded in or adhered to the surface of larger-sized particles (attributed to bonding or coalescence between small- and large-sized particles facilitated by the high process temperature). The PSD of the FBR powder was narrower than that of the as-received powder, with increased narrowness of the PSD of the FBR powder occurring with increase in T_{bed}. D_m of FBR powder was larger than that of the as-received powder, but, with processing in the FBR, D_m did not increase monotonically with T_b (**Table 1**). For the FBR powder, the change of flowability with increase in T_{bed} is complex, with flowability increasing slightly between T_{bed} = 450˚C and 500˚C but decreasing continuously between

500˚C and 600˚C (Table 1). This trend was attributed to a depreciation of the fluidized state of the powder due to moderate sintering occurring between powder particles at T_{bed} > 500˚C. The flowability of the as-received powder was not obtained because of "its extremely poor flowability" although the flowability of the FGR powder when T_{bed} = 450˚C was comparable to that of Ti powder produced using GA, GSD, or plasma atomization (PA) and possessed PSD similar to that of the as-received powder. It was thus suggested that FGR processing reduced powder flowability to a level similar to that of powders that are widely used in MAM. For the FBR powder, O content increased markedly with increase in T_{bed}, with the large proportion of the oxygen being in the powder surface and a much smaller amount uniformly distributed in the powder matrix. The trend in O content (Table 1) was consistent with the increase in the thickness of the oxide layer on the particle with increase in T_{bed}. It was suggested that FBR processing of HDH-produced powder at T_{bed} = 450˚C for 10 min yielded a powder with low enough O content (mean: 0.35 wt./wt%) and moderate enough flowability (35.2 ± 0.3 s/50g) for it to be suitable for use in MAM.

For Inconel 718, Ti-6Al-4V, AlSi10Mg, and Scalmalloy powders, the influence of the conditions in which the powder was dried prior to its use (in air, at 150˚C, for 20 min versus in vacuum, at <1 Pa, at 85˚C, for 12 h) on ρ_{app} and flowability has been reported [61]. When all the results were considered, for each of the powders, the influence of powder drying condition on ρ_{app} was marginal and flowability of Ti-6Al-4V powder decreased with drying, with the best flowability being obtained when the powder was dried in air. For each of the other three powders, the influence of drying conditions on flowability was inconsistent.

The influence of cryomilling (which is attrition ball milling in liquid nitrogen) on various properties of GA-produced 17 - 4 stainless steel powder has been studied [62]. Two groups of cryomilled powder were obtained. In one group, the powder was not degassed at the end of the process. In the other group, the powder was degassed (powder was heated, under flowing argon, from room temperature to 325˚C, at 10˚C/min, held there for 6 h, and, then, cooled to room temperature) and, then, sieved with a −325 mesh screen. In terms of morphology, most of the GA-produced powder particles were round (mean sphericity and symmetry = 0.74 and 0.91, respectively) (Table 2) and contained pores and satellite particles and some of the particles were hollow. Compared to the GA-produced powder particles, the cryomilled + degassed + sieved powder particles were less round (shaped like thin plates) and displayed noticeable increase in the sizes of the small particles (~59%), the medium particles (~40%), and the large particles (~25%) (Table 2). Both powders contained the same phases and displayed very similar melting range (1456˚C - 1474˚C) and solidification point (1455˚C ± 9˚C). The cryomilled + degassed + sieved powder had greater flowability than the GA-produced powder (~48%) (Table 2), a possible explanation for this trend being that during cryomilling, the finest particles in a powder were removed.

Table 2. Influence of cryomilling on a selection of properties of 17 - 4 stainless steel powder (results extracted from the study by Kellogg *et al.* [62]).

Condition	D_{10} (μm)	D_{50} (μm)	D_{90} (μm)	Mean sphericity	Mean symmetry	Flowability[a]
As-received (argon GA[b])	6.38	15.27	32.16	0.74	0.91	3.8
Cryomilled and degassed	10.13	21.41	40.19	0.66	0.89	2.0

[a]Unconfined failure stress at a major principal consolidation stress of 10 kPa. [b]GA: gas atomization.

For cold-spray 316L stainless steel and Cu powders subjected to high-energy ball milling, the changes in morphology and aspect ratio of the powder were influenced by the combination of ball-to-powder ratio (BPR) (1:1 - 1:10) and number of milling cycles (NMC) (2 - 30 cycles) [63]. For 316L stainless steel powder, in general, increase in BPR (for a fixed NMC) and increase in NMC (for a fixed BPR) led to flattening of the particles but with little change in morphology (the particles remained spherical). For BPRs of 1:10 and 1:5, there was practically no change in mean aspect ratio with increase in NMC; however, for BPRs of 1:1 and 2:1, there was a very gradual increase in mean aspect ratio from ~1.4 to ~2.0, with increase in NMC. The same trends were seen for Cu powder, with the difference being that flattening led to a change of spherical powder to flake-like particulates because Cu is markedly softer than 316L stainless steel.

Subjecting HDH-prepared Ti powder to ball milling led to marked changes in various powder properties [64] [65]. Compared to the as-received powder, the ball-mill-treated powder had higher O content (by ~40%) (attributed to use of Ar gas as the shielding atmosphere); improved morphology (grinding of the edges of the powder with minimal agglomeration led to a change from non-spherical to near-spherical morphology); narrower PSD; and smaller D, which was attributed to collisions and friction that occurred during the milling (D_{10}, D_{50}, and D_{90} decreased by ~49, ~20, and ~14%, respectively). In terms of microstructure, both powders had α-Ti structure but whereas the grains in HDH-produced powder were large (>1 mm) and possessed negligible microstrain, ball-mill-treated powder had a "core and shell" structure with nanocrystallites in the shell and stress-induced twins, resulting in considerable grain refinement (grain size: 92.89 ± 0.25 nm). Additionally, the ball-mill-treated powder had a lower Hauser Ratio (by ~13%), resulting in increase in flowability index (by ~8%), and displayed between small and very large changes in each of the three flowability/rheological properties determined (angle of repose decreased by ~16%, degree of compression decreased by ~12%, and specific surface area increased by ~83%).

4. Influence of Process Variables on Powder Properties

The influence of the composition of the gas used (two variants of nitrogen and Ar) in the production of AISI 316L austenitic stainless steel powder using GA

has been investigated [66]. There were three study groups, comprising powders produced using two variants of N_2 gas ("nitrogen gas A" powder (procured from one vendor) and "nitrogen gas B" powder (procured from a different vendor)) and Ar gas ("argon gas powder"). Clear trends were seen in some of the powder properties determined (**Table 3**). The powders possessed comparable values of convexity and circularity but differences were seen in aspect ratio, with 65% of the particles in the Ar gas powder falling in the range of 0.9 - 1.0 but only 55% of the nitrogen gas A particles or nitrogen gas B particles falling in that range. The PSDs of the three powders, as determined using the volume of particles, were similar but when the analysis was based on numbers of particles, there was a slightly higher number of fine particles in the Ar gas powder compared to either of the nitrogen gas powders. The highest and lowest internal porosities were found in the Ar gas and nitrogen B powders, respectively. Compared to the Ar gas powder, both ρ_{app} and ρ_{tap} for the nitrogen gas powders were lower but each of the flowability properties determined (Hausner Ratio, Hall flow rate, and angle of repose) was similar for all three powders. The avalanche angle for Ar gas powder was lower than that of either of the nitrogen gas powders, reflecting the difference in morphologies of the powders; however, some of the other rheological properties (such as specific energy (SE)) were similar for the three powders. The packing density of the Ar gas powder was higher than that of either of the

Table 3. Influence of gas used in gas atomization on a selection of properties of 316L austenitic stainless steel powder (results extracted from the study by Gao *et al.* [66]).

Property	Nitrogen gas A	Nitrogen gas B	Argon gas
D_{10} (μm)	11.8	10.1	10.8
D_{50} (μm)	23.4	21.3	19.5
D_{90} (μm)	38.0	32.1	31.9
Convexity at D_{50}	0.992	0.992	0.993
Aspect ratio at D_{50}	0.978	0.978	0.983
Circularity at D_{50}	0.911	0.914	0.940
Mean ρ_{app} (g/cm^3)	4.38	4.35	4.53
Mean ρ_{tap} (g/cm^3)	5.00	5.07	5.19
Mean Hausner Ratio	1.14	1.16	1.15
Mean Hall flow rate (s/50g)	13.3	14.3	13.1
Mean angle of repose (˚)	31.6	32.6	30.9
Mean avalanche angle (˚)	40.9	41.0	36.7
Mean specific energy (mJ/g)	2.82	2.97	3.00
Mean volume porosity (%)	4.8	3.0	5.4
Permeability, at applied normal stress = 8 kPa (10^9 cm^2)	9.0	6.5	5.8

nitrogen gas powders, a trend also attributed to differences in the morphologies of the powders. The permeabilities of these powders (a reflection of their packing structures) were in the order nitrogen gas A powder > nitrogen gas B powder > Ar gas powder.

The influence of several variables on PSD and D_m of plasma rotating electrode process (PREP)-produced Ti-6Al-4V powder has been investigated [67]. The variables were: rotation speed (7000 - 12,000 rpm), electrode diameter (15 - 25 mm), plasma current (50 - 70 A), gas (Ar and He), and gas flow rate (0, 70, 110, and 160 L/min). At a given electrode diameter, D_m decreased monotonically with increase in rotation speed, up to 10,000 rpm, beyond which the decrease flattened out. At a given rotation speed, D_m decreased with increase in electrode diameter. For a fixed combination of electrode diameter of 15 mm and rotation speed of 7000 rpm, D_m increased with increase in plasma current, attributed to increase in the size of droplets from the fluid strips and possible increased recombination of the droplets in the process chamber. Compared to when Ar gas was used, D was smaller when He gas used because of the formation of a significantly greater inclined end face of the electrode (defined as the difference between the highest and the lowest parts of the residual end face of the electrode). It was suggested that this difference may be a consequence of the difference in thermal properties of the gases: specific heat of He gas is ~10 times that of Ar gas and thermal conductivity of He gas is ~9 times that of Ar gas. In either Ar or He gas, D_m decreased with increase in gas flow rate and then increased with further increase in flow rate. This complicated pattern of variation was attributed to the disturbance and cooling effects caused by the flowing gas. Specifically, the disturbance effect, which led to a decrease of D_m, was attributed to two phenomena: first, fluid granulation caused by the fluid stream being disturbed by the mechanical crashing of the gas on it, and, second, the mechanical crushing leads to decreased number of adjacent droplets. The increase in D_m was attributed to the increased cooling rate of the molten metal. The gas flow rate at which the change of dominant effect (from disturbance effect to cooling effect) occurred was ~57% higher when Ar gas was used compared when He gas was used because the thermal conductivity of Ar gas is ~90% lower than that of He gas. The results with respect to influence of rotation speed and electrode diameter on D_m and PSD, computed using a numerical method (computational fluid dynamics), were very close to those obtained from the experimental tests.

5. Influence of Powder Production Method on Powder Properties

There is a limited volume of literature on this topic [37] [39] [68]-[73].

Two Ti-6Al-4V powders, one produced using GA (GA powder) and the other using PREP (PREP powder), were compared with respect to morphology, surface chemical composition, and PSD [68]. While both GA and PREP particles were spherical and, essentially, have the same surface compositions, distinct differences were seen in the PSDs. Specifically, GA particles were large, with a

broad size distribution (45 – 100 μm) and a large proportion of particles with D < 45 μm and a large proportion of particles with D > 55 μm, whereas PREP particles had a narrower size distribution (25 – 45 μm), a very large proportion of particles with D < 40 μm, and a very small proportion of particles with D > 45 μm.

Two Ti-6Al-4V powders, one produced using electrode induction melting gas atomization (EIGA powder) and the other using PREP (PREP powder), were compared with respect to PSD, morphology, and microstructure [69]. With regard to PSD, while EIGA powder particles distributed in five size fractions (0 - 60, 60 - 80, 80 - 120, 120 - 180, and 180 – 250 μm; D_{50} = 93 μm), PREP particles distributed mainly in only two size fractions (80 - 120 and 120 – 180 μm; D_{50} = 135 μm). EIGA powder particles were nearly spherical with several satellites, and had sub-grains that resulted in the formation of a cellular microstructure (especially in the larger-sized particles), a consequence of rapid cooling experienced during the powder production process. PREP powder particles were entirely spherical, smooth, and free of satellites, with sub-grains seen only in a small proportion of the particles. In both powders, the particles were composed of martensitic α' phase, a consequence of the very high cooling rate experienced during each powder production process (on the order of 10^3 - 10^5 K/s).

Various properties of Ti-6Al-4V powders produced using three different methods were compared [70]. The methods were PA (PA powder), GA (GA powder), and PREP (PREP powder). The properties determined were morphology (through the use of scanning electron microscopy (SEM) and synchrotron x-ray computed tomography (SXRCT)), PSD, O content, flowability, ρ_{app}, pore morphology within the powders, and porosity (**Table 4**). SEM showed that although each powder was spherical, PREP powder showed the highest surface smoothness and sphericity. While the PSDs of PA and GA powders were similar (characterized by bi-modal peaks), that of PREP powder was distinctly different (showing only one peak). PA powder had the smallest O content, but the flowabilities of the three powders were about the same, with the same trend found for ρ_{app}. SEM results showed that while pores ranging in D from 10 – 50 μm were found in GA and PA powders, no pores were found in PREP powder. SXRCT results showed that there were more satellites in GA powder than in either PA or PREP powders, quasi-spherical pores in GA and PA powders, irregularly-shaped pores in PREP powder, and internal pores in all three powders but more in GA and PA powders, with the smallest and largest internal pore sizes being found in PA and GA powders, respectively. For powders with D < 150 μm, mean porosity was in the order GA powder >> PA powder >> PREP, with the same trend seen in the mean Ar contents. Porosity increased with increased D, with the patterns for PA and PREP powders being the same (that is, monotonic increase). For each powder, Ar content increased with increase in D. Clear differences between the powders were seen in the variation of pore porosity: broadly speaking, at each D, porosity was in the order GA powder > PA powder > PREP powder. Results for variation of pore sphericity with D showed sphericity in the order GA

Table 4. Influence of powder production method[a] on a selection of powder properties[b].

Powder	O (%)	D_{10} (μm)	D_{50} (μm)	D_{90} (μm)	Circularity index	ρ_{app} (g/cm^3)	ρ_{tap} (g/cm^3)	Porosity (%)	Flowability (s/50g)	HR	CI	AMS	Ref.
Ti-6Al-4V alloy													Chen *et al.* [70]
GA	0.12	43	70	98		2.38	0.20		33.5				
PA	0.08	42	60	92		2.59	0.12		31.8				
PREP	0.10	40	105	120		2.59	0.08		29.6				
Ni-based 625 alloy													Mostafaei *et al.* [37]
GA		19.7	28.2	63.1	0.957			2.4					
WA		20.2	42.1	42.1	0.755			3.0					
Ti-6Al-4V alloy													Sun *et al.* [71]
GA[c]	1292 ± 420 ppm		76 ± 27[d]			2.48 ± 0.06	2.83 ± 0.07		26.14 ± 0.82				
PREP	2010 ppm		82 ± 25[e]			2.63 ± 0.00	2.78		26.78 ± 0.09				
Ti-6Al-4V alloy													Brika *et al.* [72]
GA		25.3	35.8	46.4	0.79	2.39	2.55		35	1.07	1.05	0.975	
PA		20.3	32.7	43.9	0.84	2.58	2.70	0.12	26	6.27	4.44	0.759	

[a]GA: gas atomization; PA: plasma atomization; PREP: plasma rotating electrode process; WA: water atomization. [b]HR: Hausner Ratio; CI: Carr Index; AMS: additive manufacturing suitability index. [c]5 variants, as purchased from 5 different vendors. [d]Mean and population standard deviation of all the D_{10}, D_{50}, and D_{90} results for all 5 variants of GA-produced powder (Camsizer® results). [e]Mean and population standard deviation of all the D_{10}, D_{50}, and D_{90} results (Camsizer® results).

powder > PA powder > PREP powder. The difference in sphericity between the different powders was attributed to differences in pressures of the gas trapped within the particles during the atomization process (~five times lower in the case of PREP powder particles compared to the case in both GA and PA powder particles). For each of the powders, three-dimensional (3D) reconstructed images obtained using SXRCT showed that the pore population increased with increase in D.

A comparison between GA- and water atomization (WA)-produced Ni-based alloy 625 powders was carried on the basis of morphology, structure, PSD, composition, and particle porosity [37]. GA powder was spherical whereas WA powder particles were angular and irregular in shape. In both powders, the particles had a dendritic microstructure. The mean O content of GA powder was ~99% lower than that of WA powder, with a similar trend seen for the C content

(~55% lower). For each of the crystallographic parameters determined, the values for the two powders were essentially the same. In differential scanning calorimetry tests, melting began in GA powder at 1304˚C and ended at 1334˚C whereas for WA powder, the corresponding temperatures were 1252˚C and 1305˚C, respectively, which indicated that the solidus temperature (T_{sol}) of GA powder was about 52˚C higher than that of WA powder. The difference in T_{sol} between the two powders was attributed to the GA powder having a lower C content. For GA powder, its PSD was wider, D_{50} was smaller, circularity was greater, and % mean porosity was lower compared to the corresponding values for WA powder (**Table 4**).

For Ti-6Al-4V alloy powder produced using PREP and 5 "variations of the gas atomization (GA) process", PSD (obtained using SEM and a commercially-available particle size analyzer (Camsizer®)), morphology (using SEM, back-scattered electron SEM (BSE-SEM), and transmission electron microscopy (TEM)), microstructure, chemical composition, PSD, flowability, ρ_{app}, and ρ_{app} were obtained [71]. The variations in GA-produced powders reflect differences in processing conditions used by the 5 different vendors from whom the powders were procured (AP & C, ATI, Hoeganaes, Praxair, and Puris). In terms of PSD, PREP powder had a uni-modal distribution, each of 2 of the variants of GA powders had bi-modal distribution, and each of the other 3 variants of GA powders had discontinuous distribution. Camsizer® analysis results gave the range of D for PREP powder as 52 – 114 μm, while, among the 5 GA powders, there were differences seen in this range (for 1 variant: 38 – 102 μm and for another variant: 57 – 95 μm). Mean D_{50} for GA powders was considerably lower (~30%) than that of PREP powder (**Table 4**). For some of the powders, the PSD results from SEM and Camsizer® analyses were the same; for example, for one GA variant powder, very few particles were detected at D > 120 μm. However, for other powders, the PSD results obtained using SEM and those obtained using Camsizer® were different; for example, for PREP powder, D_{50} was 64 mm and 79 μm from SEM and Camsizer® analyses, respectively.

In terms of morphology, PREP powder particles were spherical and had smooth surfaces; particles of Puris powder were less smooth than PREP ones and had satellite particles attached to many of the larger particles and not all of them were spherical; and particles of Praxis powder were, mostly, spherical, with some that were elongated.

With respect to microstructure, particles of each of the powders exhibited only the peaks associated with HCP a (or α') phase, an acicular α' martensite microstructure with lath thickness of ~200 nm, and twins within the laths.

In terms of chemical composition, PREP powder had the highest mean O content, while, among the variants of PA powder, the mean content in Praxair and AP&C powders was markedly lower than that in the 3 other variants. Among all the powders, Ti, Al, and V contents were, essentially, the same. The flowability of PREP powder was within the range of that of the 5 variants of GA powder, with the same trend seen for ρ_{app} and ρ_{tap} (**Table 4**).

The morphology, PSD, porosity, and rheological properties of PA- and GA-produced Ti-6Al-4V alloy powders have been compared [72]. In terms of morphology, PA particles were spherical, whereas GA powder particles were irregularly shaped. Clear differences between the particles from these two powders were seen in sphericity, PSD, ρ_{app}, ρ_{tap}, flowability, Hausner Ratio, and Carr Index (**Table 4**). Additionally, these workers [72] introduced a figure of merit (AMS) as a measure of the suitability of a powder for use in an LB-PBF process. AMS was calculated as the arithmetic mean of the 7 rheological properties of the powder that were determined. AMS of PA powder is ~28% lower than that for GA powder (**Table 4**). It was postulated that the smaller AMS is, the greater is the suitability of the powder for an LB-PBF process. As such, it was suggested that PA powder was more suitable than GA powder.

3D size, shape, and internal porosity of particles of recycled Ti-6Al-4V powders that had been produced using PA and GA were determined [39]. This was achieved by use of a methodology that involved use of x-ray computed tomography (XCT) and various mathematical algorithms. The methodology was calibrated by limited visual examination of 3D images of individual particles, which allowed classification of the particles as either nearly spherical (SnS) or non-spherical (NS). The latter type can be single non-spherical particles or multi-particles (comprising 2 or more conjoined particles). Clear differences were seen between the powders in terms of the particle shape classification (**Table 5**), showing that the sphericity of the PA powder particles was greater than that of the GA powder particles. However, the various aspect ratios of the two powders were comparable (**Table 5**) as were the various PSDs (that is, those based on W and VESD), L/T, L/W, and W). The superior quality of PA powder was also seen in the porosity results (**Table 5**).

For PA- and HDH-produced Nb-47Ti powders, clear differences were seen in each of the properties determined, with one exception [73]. PA powder particles were spherical, had mean ρ_{app} of 3.45 g/cm^3, Hall flowability of 20 s/50g, and mean O content of 0.12 wt./wt%, whereas HDH powder particles were irregularly shaped, had mean ρ_{app} of 1.85 g/cm^3, no measurable flowability, and mean O content of 0.34 wt./wt%. The exception was that the PSDs of the powders were similar. There was no discussion of these results except to show that the effective

Table 5. Influence of powder production method on a selection of properties[a] of recycled Ti-6Al-4V alloy powder (results extracted from the study by Garboczi and Hrabe [39]).

Production method	% SnS particles	% NS particles	AR (L/T)	AR (W/T)	AR (L/W)	Mean porosity of all particles (%)
GA	38.4	61.6	1.39	1.11	1.25	0.19
PA	71.5	29.2	1.38	1.10	1.25	0.077

[a]SnS particles: particles that are nearly spherical; NS particles: particles that are not spherical; AR: aspect ratio; L: length of particle; T: thickness of particle: W: width of particle.

layer thickness (ELT) of the deposited powder in an LB-PBF process (defined as the height that the powder must fill due to the solidification shrinkage of the powder bed and the displacement of the build platform) is inversely proportional to ρ_{app} of the starting powder. Using PA powder in an LB-PBF process with volumetric energy density of 79 ± 16 J/mm^3, the calculated ELT was 53 μm, whereas using HDH powder in the same process with volumetric energy density of 40 ± 8 J/mm^3, the calculated ELT was 200 μm.

6. Influence of Powder Reuse on Powder Properties

Although the majority of the studies on this topic have been on Ti-6Al-4V alloy powder [74]-[87], a variety of alloy powders, namely, Ni-based alloys [82] [86] [88]-[95], stainless steels [96]-[102], and Al-based alloys [82] [101] [103] [104] [105] [106], have also been studied.

For Ti-6Al-4V alloy powders intended for SLM and EB-PBF, powder reuse has a very marginal influence on PSD and aspect ratio [75]. With respect to flowability of the powder intended for EB-PBF, powder reuse impaired flowability (higher SE, higher basic flow energy (BFE), lower conditioned bulk density, and lower flow energy after 50 taps). The opposite outcome was found for the powder intended for SLM.

For ELI Ti-6Al-4V powder, the influence of reuse of the powder (up to 21 cycles) on O content, particle morphology, PSD, flowability, ρ_{app}, and ρ_{tap} has been determined [76]. With increase in the number of reuse cycles, O content increased in a monotonic manner, the PSD became narrower although there was very little change in D_{50} (**Table 6**); the powder particles became less spherical and rougher, distorted after the 16th and 21st reuse cycles (**Figure 7**); satellite particles were visible after the 2nd and 6th reuse cycles but there were few of these after the 11th reuse cycle (**Figure 7**); flowability improved by a modest amount in that the flow rate increased by ~12%, ρ_{app} remained about the same, and ρ_{tap} decreased by ~3% (**Table 6**). The following explanations were given for these trends: increase in O content was due to pick-up of oxygen when the powder was exposed to air, including when the unmelted powder was blown off from the part being built. As for the narrowing of the PSD, during the time that the unmelted powder was blown from a part being built, and, then, collected, some satellite particles became detached from the parent particle and was carried away by the gas being used in the MAM process. Improved flowability was not consistent *with a priori* expectation and was attributed to the removal of satellites from the particles and a reduction of moisture in the powder after prolonged exposure to vacuum, at elevated temperature, in the build chamber machine.

For PA-produced Ti-6Al-4V powder, powder reuse (up to 7 cycles) yielded changes in the phases in the powder [77]; namely, α or martensitic α' in the virgin powder; β phase after the 1st and 2nd cycles; α phase boundary after the 3rd cycle; near-equiaxed prior β grains and phase boundary after the 4th cycle; and

Table 6. Influence of powder re-use on a selection of powder properties[a].

Powder	O content (wt./wt.%)	Flowability (s/50 g)	AA (˚)	AE (mJ/kg)	DD (g/cm^3)	ρ_{app} (g/cm^3)	ρ_{tap} (g/cm^3)	D_{10} (μm)	D_{50} (μm)	D_{90} (μm)	Ref.
Ti-6Al-4V											Tang *et al.* [76]
Virgin	0.08	32.47				2.56	2.96				
10 cycles	0.17	29.50				2.58	2.94		72.7[b]		
21 cycles	0.19	28.34				2.57	2.88		73.2[c]		
Ti-6Al-4V											Denti *et al.* [81]
Virgin		1.59						24.6	38.6	59.9	
100 cycles		3.42						19.7	30.6	47.3	
Inconel 718											Paccou *et al.* [93]
Virgin			51.8	22.11		4.50	5.26	14.6	27.1	49.0	
50 cycles		16.16	44.3	11.91		4.35	5.12	19.2	30.8	49.6	
ATI 718											Rock *et al.* [94]
Virgin	135 ppm	11.5						26.5	31.5	49.3	
5 cycles	215 ppm	12.3						26.5	40.1	72.3	
9 cycles	270 ppm	13.5						24.3	40.2	84.6	
AISI 304L stainless steel											Sutton *et al.* [99]
Virgin	248 ppm		34.8	8.42	4.41	4.35	4.72				
4 cycles	313 ppm										
7 cycles	335 ppm		33.3	7.20	4.50	4.45	4.80				
AISI 316L stainless steel											Yusuf *et al.* [101]
Virgin	1.42								22.0		
50 cycles	4.68								29.0		
AlSi10Mg alloy											Yusuf *et al.* [101]
Virgin	1.49								11.0		
50 cycles	3.01								13.0		
AISI 316L Stainless steel											Heiden *et al.* [98]
Virgin	0.067 ± 0.010							7.0	16.9	26.9	
30 cycles	0.095 ± 0.014							8.2	15.4	27.5	

[a]AA: avalanche angle; AE: avalanche energy; DD: dynamic density. [b]After 2 reuse cycles. [c]After 16 reuse cycles.

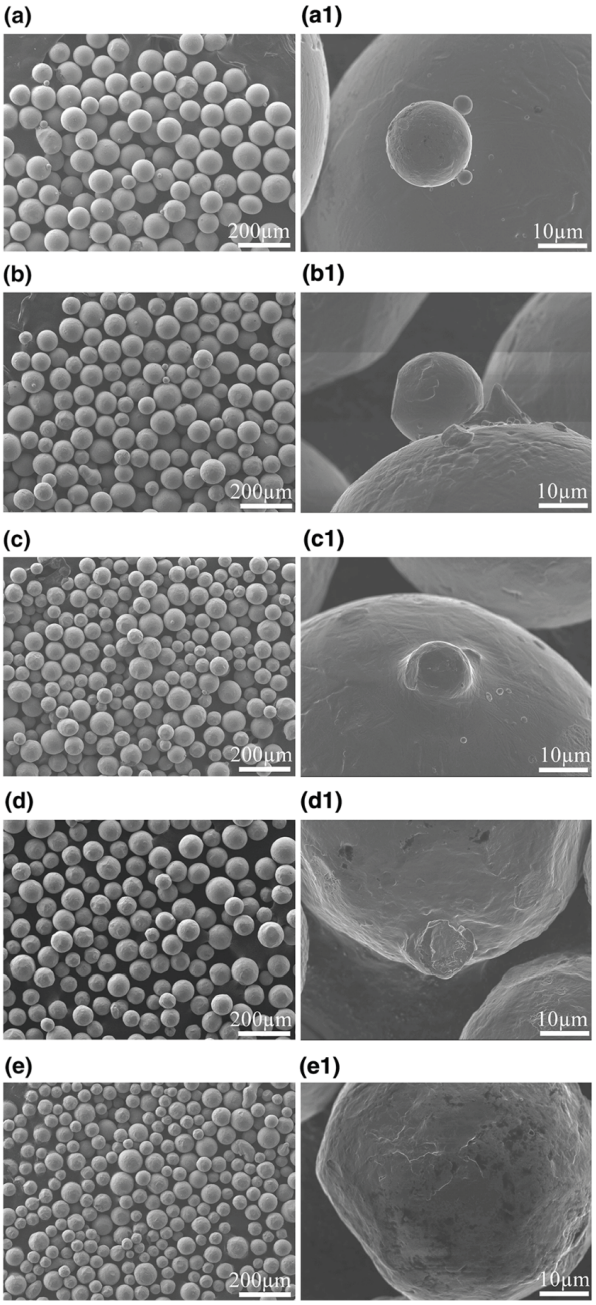

Figure 7. Morphology and surface features of reused Ti-6AI-4V alloy powder, with number of times of reuse being 2 (a), 6 (b), 11 (c), 16 (d), and 21 (e) [76].

two types of transformed α and β duplex microstructure with lamellar colony and Widmanstatten microstructure after the 7th cycle. Regardless of the number of reuse cycles, most of the peaks in the x-ray diffraction (XRD) profile of the powder originated from the HCP phase, and the peak width decreased with increase in number of reuse cycles, which was attributed to improved crystallinity that accompanied the re-heating and re-cooling processes. With increase in the number of reuse cycles, the trends were: increase of O content of the powder (mean increase of ~25% after the 7th reuse cycle compared to the value for the

virgin powder), increase of the microhardness of the powder (mean increase of ~29% after the 7th reuse cycle compared to the value for virgin powder), and increase of the elastic modulus of the powder (mean increase of ~24% after the 7th reuse cycle compared to the value for virgin powder).

For Ti-6Al-4V [78], with reuse (over a maximum of 69 cycles), the change in the Ti, Al, and V contents was each negligible, but the O content increased progressively; and the particle morphology changed from spherical (virgin powder) to one that contained a variety of defects, such as elongated particles, bonded and agglomerated satellites, and satellites with particles, a consequence of the sieving procedure and overheating and smelting.

For ELI Ti-6Al-4V alloy powder, reused powder had higher O content and essentially unchanged nitrogen content [79]. Additionally, with increase in number of builds (1 - 31), the PSD became narrower, with no change in D_{10} or D_{50} but decrease in D_{85}; the particles remained essentially spherical but coarser and there were fewer satellites; ρ_{tap} decreased; and flowability improved (as a result of decreased number of satellites).

For GA-produced Ti-6Al-4V alloy grade 23 powder [80], after 15 reuse cycles, the PSD narrowed, with D_{10} being approximately unchanged, D_{50} being slightly smaller, and D_{90} being markedly smaller; the particles remained spherical, with fewer satellites; O content increased while nitrogen content was unchanged; flowability improved (markedly lower BFE and markedly lower permeability); and thermal conductivity increased.

For Ti-6Al-4V powder [81], the virgin powder particles were nearly spherical and contained a few slightly elongated particles and a few broken particles, and were fully dense, with a feather-like microstructure. In the powder after the 100th reuse cycle, there were satellite particles attached to the powder surface and a few aggregates. Powder reuse led to narrowing of the PSD, decrease in D_{50} (~21%), and a large drop in flowability (~54%) (**Table 6**).

In the case of PA-produced Grade 5 Ti-6Al-4V powder [83], the virgin powder particles were smooth, with a high degree of sphericity and comprised a large range of particle sizes, satellite particles that adhered to the larger-sized particles, and a number of non-spherical particles. With increase in the number of reuse cycles (up to 30), the particles became more irregularly shaped, there was increase in particle surface damage, the number of smaller-sized particles decreased, and the PSD narrowed (from a bimodal distribution and tended to a Gaussian distribution after the 30th reuse cycle), with the trends in D_{10}, D_{50}, and D_{90} being small increase, no change, and marked decrease, respectively. As for chemical composition, the O content increased markedly with increase in powder reuse cycles, with the content after the 11th cycle exceeding the ASTM F2924 limit [84] (0.2 wt./wt%). Most likely, the surface damage to the particles occurred during powder handling and recovery. Decrease in the number of small-sized particles may be the consequence of them being consumed during part building, fused onto the surface of larger-sized particles, or lost during powder recovery. This decrease may be the reason for the trend in D_{10} while the

trend in D_{90} may be accounted for by size of the sieve used to collect the used powder (120 sieve), which removed powder particles and agglomerates with size > 125 μm.

For PA-produced Grade 5 Ti-6Al-4V alloy powder intended for use in EB-PBF, the influence of powder reuse on a very wide collection of powder properties, including D_{50}, r_{tap}, O content, and various measures of flowability (such as Hausner index and angle of repose), has been determined [87]. Seven powder groups were used; however, for three of them, it involved mixture of virgin and used powder and, as such, results for those powders are not summarized here. Thus, the four groups focused on here are virgin powder (G_0 powder), powder reused after 1 build cycle (G_1 powder), powder reused after 2 build cycles (G_2 powder), and powder reused after 3 build cycles (G_3 powder). Clear changes were seen in the morphology of the powder (for example, satellites in G_o powder, particles with molten specks in G_2 powder, and shattered particles in G_3 powder) and in most of the other powder properties determined (**Table 7**). In addition to a discussion of the trends for each of the properties determined, the authors calculated the arithmetic mean of the values of the 13 properties determined and designated this parameter as the electron beam powder bed fusion suitability factor (ESF). The authors postulated that the closer this factor is to that for the virgin powder, the more the suitable is the powder for use in an EB-PBF method. There was clear demarcation between the ESF of the virgin powder, on one hand, and ESFs of the three reused powders, on the other; additionally, ESF increased monotonically with increase in number of reuse cycles (**Table 7**).

In the case of IN718 powder [90], compared to virgin powder, reused powder showed noticeable increases in D_{10}, D_{50}, and D_{90}; slight decreases in ρ_{app}, ρ_{tap}, and ρ_{true}; marginal depreciation in flowability (small increase in time in the Hall flow test); and better rheological properties (for example, increased BFE, flow rate index, SE, and compressibility). The decreased flowability of the reused powder was attributed to distortion of the shape of the particles over time, resulting in them no longer being spherical.

Table 7. Influence of powder reuse on a selection of properties[a] of plasma-atomized Ti-6Al-4V alloy powder (results extracted from the study by Shanbhag and Vlasea [87]).

Powder	O content (wt./wt%)	D_{10} (μm)	D_{50} (μm)	D_{90} (μm)	ρ_{tap} (g/mL)	ρ_{bulk} (g/mL)	HR	CI	SE	ESF
Virgin	0.130	48	66	95	2.83	2.67	1.06	5.35	1.48	0.176
1 cycle	0.158	47	62	93	2.85	2.67	1.07	6.20	1.60	0.504
2 cycles	0.176	51	65	95	2.88	2.66	1.08	7.20	1.62	0.609
3 cycles	0.178	49	70	100	2.92	2.68	1.09	8.10		0.659

[a]HR: Hausner Index: CI: Carr Index; SE: specific energy; ESF: electron beam powder bed fusion suitability factor.

Inconel 718 and Ti-6Al-4V powders were the subject of one study [86]. For Inconel 718 powder, with increase in the number of powder reuse cycles, there was minimal change in particle shape, increase in particle agglomeration (attributed to slow sintering in the powder mound in the additive manufacturing machine), slight narrowing of the PSD but not in a systematic manner, increase in the number of large-sized particles, and increase in $D_{50.}$ For Ti-6Al-4V powder, there was also an increase of D_{50}, but there was slight broadening of the PSD, and fast sintering led to large particles being sieved out at the end of each build, resulting in fewer sintered agglomerated particles.

For GA-produced Inconel 718 powder, powder reuse (up to 50 cycles) led to various changes in powder properties [93]. O content markedly increased (by ~85%) to a level that was still below that specified for use of this powder for additive manufacturing of parts for aeronautical applications. There was noticeable change in PSD (for example, increased D_{10}, D_{50}, and D_{90} (**Table 6**)) and decreased circularity. Increase in particle sizes was attributed to the presence of spatters and satellites in the reused powder. Both ρ_{app} and ρ_{tap} of the reused showed very small decreases (~3% in each) and, hence, flowability increased (**Table 6**). It was suggested that the increased flowability may be linked to the decreased amount of small particles in the powder or particle oxidation.

For GA-produced nickel superalloy ATI 718 powder [94], powder reuse (up to 9 cycles) led to changes in particle size and morphology of the powder. Specifically, the number of large-sized particles increased and many of these particles had non-spherical agglomerated or fused particle morphologies, the PSD flattened, and O content increased considerably (by a factor of ~2) (it was suggested that the presence of features, such as films and spots, which consisted of Al oxides, may contribute to this increase), D_{50} increased (by ~28%), and flowability decreased (by ~15%) (**Table 6**).

In the case of GA-produced IN718 powder [95], with increase in powder reuse (between 1 and 14 times), the bulk composition of the powder was, practically, unchanged; the PSD shifted to the right (meaning that D_{10}, D_{50}, and D_{90} increased, with these increases being marked after the 14th reuse); the volume fraction of small-sized particles ($D < 25$ μm) decreased, but that of particles with $D > 35$ μm increased; the particles remained, more or less, spherical with some satellites but the number of satellites decreased (**Figure 8**); and both ρ_{app} and flowability increased, which was attributed to decrease in the volume fraction of small-sized particles, which limited the formation of agglomerates.

For Ar gas atomized-produced 17 - 4 precipitation-hardened stainless steel powder, with increase in number of builds (1 - 14) [97], three findings were 1) very small narrowing of PSD, very small decrease in the circular equivalent diameter of the particles, increases in both ρ_{app} and ρ_{tap}, with all these changes being a consequence of the existence of fewer large agglomerates in the reused powders; 2) practically no change in the shape morphology of the particles, with them remaining spherical or near spherical; and 3) marked decrease in compressibility,

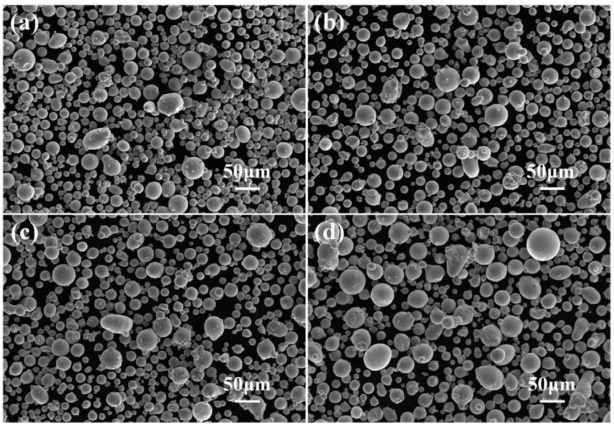

Figure 8. Morphologies of reused Inconel 718 alloy powder, with number of times of reuse being 2 (a), 6 (b), 10 (c), 14 (d) [95].

decrease in permeability, and increase in flowability, trends that were attributed to reduction of the amount of empty spaces in the powder.

Various properties of virgin and reused (up to 30 cycles) 316L stainless steel powders were compared [98]. With reused powder, there was a marked increase in the bulk concentration of O (by ~42% (**Table 6**), small widening of the PSD (**Table 6**), small reduction of circularity, small reduction of aspect ratio, and small increase of nanohardness (NH) of the particles. For each of the powders, particle shapes included spherical, angular/irregular, and rod-like, with satellites (nm- to μm-sized) for both virgin and reused powders, but, with reuse, the proportion of irregular-shaped particles increased slightly. There were distinct grain boundaries on virgin powder particles whereas reused powder particles were slightly deformed and, hence, no grain boundaries were visible. With reuse, there was decreased surface roughness of the particles that did not contain satellites (postulated to be due to loss of dendrite exteriors) and a slight decrease in surface O content. In terms of crystal structure, both virgin powder and reused powders were composed primarily of γ face-centered-cubic (FCC) austenite phase with a small amount of δ body-centered-cubic ferrite phase. Reused powder had a large amount of small d ferrite grains and a large amount of fully ferritic, highly spherical particles (diameter: 5 – 50 μm). With powder reuse, the grain size of the particles decreased slightly, and NH of the particles increased slightly, particularly with increasing depth of measurement. Both sieved and reused powders contained a certain amount of full oxides, carbon-based agglomerates (soot), fume oxides, and Al-based impurities, which were created during the powder production method (atomization) or as a result of the interaction of the particles with the laser during the building of parts (LB-PBF process).

For GA-produced AISI 304L stainless steel powder [99], compared to virgin powder, recycled powder was more spherical, had noticeably higher O content (~35%), and displayed very small increases in both ρ_{app} and ρ_{tap} (~2% for each parameter), and increased flowability (for example, ~14% in decrease in avalanche energy) (**Table 6**). With increase in the number of reuse cycles, there was

a small amount of both coarsening of the powder particles and increase of the aspect ratio of the particles. In terms of morphology, clear differences were seen in the powder after the 7th reuse cycle compared to the virgin powder; namely, recycled powder contained large-sized particles, some of which were highly spherical and others that were irregular.

For GA-produced 316L stainless steel powder, influence of powder reuse on PSD, porosity, pore composition, NH, and effective modulus (E_r) of the particle was determined [100]. Compared to the virgin powder, the reused powder (over the course of 10 printing cycles) displayed about the same "average" particle size, a larger number of small-sized particles, a broader pore size distribution, a slightly reduced pore size (by ~10%), higher pore density, higher Fe, Cr, and Ni contents on the interior wall of the pore, higher Mn, S, and Si contents in the outer layer around the pore and on the surface of the particle, and lower NH and higher E_r (at a given depth of indentation). The larger number of small-sized particles was explained by their being blown away during the LB-PBF process (SLM). Higher pore density was attributed to the redistribution of the composition of the alloy powder during SLM, while the reduced NH and increased E_r was attributed to the increased porosity of the particles.

For GA-produced AISI 316L stainless steel powder [102], with reuse (up to 15 printing cycles), O content increased markedly (by ~37%), D increased slightly (for example, D_{50} decreased by ~9%; with some irregular-shaped particles seen), and flowability increased slightly (flowability time decreased by ~10%, which was attributed to decreased number of small-sized particles (which results in a reduction of interparticle separation) and increased number of particles whose surface was oxidized).

For AlSi10Mg_200 alloy powder [103], powder reuse did not affect particle morphology (spherical or near spherical, a few particles with rounded oblong shape, and a few satellites); surface finish (smooth); D_{50} (~9 μm); microstructure (the silicon phase was distributed in the dark Al matrix in the form of a bright network of plates/islands that have thin and long arms around them); and phase composition (no shifting of Al peaks).

For AlSi10Mg alloy powder [105], with increase in number of builds (up to 8), the PSD shifted slightly to the left, indicating reduction of the larger-sized particles, with no change in D_{10}, no change in D_{50}, and a slight decrease in D_{90}; the particles remained predominantly spherical; and there was a very small increase in ρ_{app} and a modest increase in ρ_{tap}.

The morphology, PSD, circularity, chemical composition, and phase (crystal structure) of virgin powder and reused powders (50 cycles) of 316L stainless steel and AlSi10Mg intended for use in an LB-PBF process were compared [101]. For each of the powders, with reuse, PSD shifted to slightly higher values (**Table 6**). For 316L stainless steel powder, both virgin and reused powder particles were largely spherical or near-spherical, but there were satellites in the virgin powder. The morphologies of the virgin and reused AlSi10Mg powders were the same,

except for the presence of satellites in the reused powder. While mean circularity of 316L stainless steel powder was, practically, unchanged with reuse (mean reduction ~2%), there was a larger decrease in that parameter in the case of AlSiMg10 powder (mean decrease ~17%). Each of the recycled powders retained its chemical composition, but with increased O content (by ~230% and ~102% for 316L stainless steel and AlSi10Mg powders, respectively (**Table 6**)). For each of the powders, powder reuse did not affect its microstructure (in the case of 316L stainless steel, a single γ-austenite FCC structure) and there were no precipitates and oxide layers. Because of the increase of O content in the recycled powder, which is often associated with the presence of contaminants inside the build chamber, it was noted that even though no phase change was observed in the XRD spectra, change that was below the limit of detection of the XRD equipment used in the study could not be ruled out. Furthermore, in the case of 316L stainless steel, the presence of nitrogen in the build chamber may mask the formation of other phases in the reused powder because nitrogen is an austenite stabilizer.

The influence of powder reuse on the morphology, composition, density, and flowability of GA-produced Ti-6Al-4V, Inconel 718, AlSi10Mg, and Scalmalloy powders has been determined [82]. With powder reuse, Ti-6Al-4V alloy powder particles remained essentially rounded and regular (no change in circularity parameter (f_{circ}) = 0.88)), Inconel 718 alloy powder particles showed decrease in circularity (f_{cir} = 0.85 and 0.79 for virgin and reused powder, respectively), AlSi10Mg powder particles showed a very small decrease in circularity (f_{circ} = 0.78 and 0.75 for virgin and reused powder, respectively), and Scalmalloy powder particles showed a very small decrease in circularity (f_{cir} = 0.83 and 0.80 for virgin and reused powder, respectively). For each of the powders, with increase in the number of reuse cycles, there was increase in the number of satellites and roughness (attributed to the remelting during part building using an LB-PBF method). Change in PSD curves for Ti-6Al-4V alloy and Inconel 718 powder particles were steeper than those for each of the other two powder particles. D_{50} was ~38.5 μm for AlSi10Mg but was ~35 μm for each of the other powder particles. There was some discrepancy in the trends in O contents of the powders between those determined using a gas analyzer (per ASTM E1409 [107]) and those determined using electron dispersion spectrometry, with the workers' conclusion being that the increase in this content with powder reuse was only found for AlSi10Mg powder. With regard to changes in microstructure brought about by powder reuse, slight remelting was observed in reused Ti-6Al-4V, Inconel 718, and AlSi10Mg powder particles but there was agglomeration in reused Scalmalloy alloy powder particles. It was postulated that these microstructural changes reflected the influence of remelting and powder alloy composition. For Ti-6Al-4V, Inconel 718, and Scalmalloy powders, powder reuse exerted a very marginal influence on ρ_{tap} but modestly enhanced flowability of each of the powders, especially in the case of Ti-6Al-4V powder (~16% increase) and Al-

Si10Mg powder (~25% increase).

Very limited attention has been given to characterizing the physical degradation suffered by a metal powder over the course of reuse [85] [92] [106]. In each of these referenced studies, the degradation was monitored by using x-ray photoelectron spectroscopy to determine the thickness of the oxide on the particle, and consistent results were obtained. With powder reuse, the thickness increased (mean of ~16% in the case of Ti6Al-4V over 10 reuse cycles [85] and mean of ~850% in the case of AlSi10Mg powder over a reuse period of ~30 months [106]). This trend was consistent with the trend that for a combination of either alloy powder and reuse duration, O content of the powder increased markedly [92] [106].

From the review of the studies on Ti-6Al-4V powder, one noticeable feature is that while in some studies, it was found that with reuse, D_{50} either decreased or was, essentially, unchanged [79] [80] [81] [83] (after between 15 and 100 cycles), in other studies, an increase (after 12 cycles) was found [74] [86]. From the review of studies on Ni-based alloys, one consistent trend is that for a given alloy, with powder reuse (over the range of up to 9 cycles and up to 50 cycles), D increased, regardless of the specific parameter considered (for example, D_{50} [86] [88] [90] [93] [94] [95] or "weighted average" [89]). Review of studies on stainless steel powders show that a wide assortment of powder properties was determined. Thus, in addition to those that are commonly determined, such as PSD, microstructure, O content, microstructure, and flowability, there were others, such as NH, and E_r [97]-[102]. For AlSi10Mg alloy powder, very few replication studies were conducted that involved the same powder property (for example, D_{50}), making it difficult to identify consistent trend(s) [103] [104] [105].

Considering all the results summarized in this Section, there is little consistency in the trends of the properties that were most commonly determined (**Table 8**). "Consistency" is herein taken to be the same direction of a trend, as

Table 8. Summary of trends in properties of influence of powder reuse on four properties of metal powders[a,b].

Alloy	Number of studies reviewed	Trend in			
		O content	D_{50}	Circularity	Flowability rate
Ti-6Al-4V	10	↑ ↑ ↑~	↑ ↓~	~	↑ ↑ ↓
Ni-based alloys (Inconel 718 and AT1718)	6	↑ ↑ ↑~	↑~	↑ ↓ ↓	↑ ↓
Stainless steels (316L, 304, and 17-4)	7	↑ ↑ ↑ ↑		↓~	↑ ↑~
Al-based alloys (AlSi10Mg and Scalmalloy)	5	↑~	↑~~	↑ ↓	↑ ↑

[a]Compared to value for the virgin powder. [b] ↑: increase; ↓: decrease; ~: practically unchanged.

reported in 5 or more studies on the same metal powder. In fact, the only consistent trend is that for Ti-6Al-4V, Ni-based alloys, and stainless steels, the O content of the powder increases markedly with powder reuse.

7. Appraisal of the Literature

In this Section, a number of shortcomings of and gaps in the literature are highlighted.

First, although extensive and detailed characterizations of powder particles have been conducted (**Table 9**), there is scope for more widespread use of more advanced characterization techniques such as synchrotron x-ray computed tomography scanning (SXCTS) for 3D reconstruction of the particles [70]; SXCTS and mathematical analysis for determination of aspect ratio of particles [39]; and synchrotron-based hard x-ray photoelectron spectroscopy for determination of the chemical composition across particle pores [100].

Second, a persistent shortcoming in the reports is the absence of statistical analysis of the results obtained. As a consequence, in reports of studies that involved comparison of two or more groups (for example, properties of GA- versus PA-produced powders for a given alloy powder and influence of powder reuse on properties of a specified alloy powder), the stated conclusions are not evidence-based. To rectify this issue, it must be ensured that non-parametric method(s) of significance testing are used. Examples are the Kruskal-Wallis test coupled with a *post hoc* test (such as the Bonferroni method), the Jonckheere-Terpstra test, and the Mann-Whitney U test.

Third, there are two common deficiencies involving information about the powder production method used in the studies. One, in some reports, the method was not stated, examples being some reports on Ti-6Al-4V alloy [75] [76] [78] [79] [81]. Two, in many reports in which the powder(s) were produced using GA, the specific variant of GA was not stated, examples being reports on Ti-6Al-4V [70] [72] [82], Inconel 718 [82], AlSi10Mg [82], Scalmalloy [82], and AISI 316L stainless steel [102].

Fourth, there is inconsistency/confusion in the use of the concept of "powder reuse". For some workers, this meant collecting all the powder left after a build was complete ("residue powder"), passing it through a sieve (typically, ≤150 μm), and using it to fabricate the next build [76] [79] [81] [86] [94] [97] [99] [102] [104] [106]. This approach is herein designated "recycled powder use". For other workers, they collected the residue powder, passed it through a sieve (typically, ≤150 μm), added it to the powder remaining in the hopper/feed bin, and, then, used this powder mixture to fabricate the next build [77] [80] [81] [82] [83]. This approach is herein designated "refreshed powder use". For a third group of workers, descriptions on how powder reuse was achieved were either unstated or were vague [75] [78] [90] [93] [95] [98].

Fifth, regardless of how powder reuse was defined in a given study, there is confusion as to what constitutes a powder reuse cycle because an assortment of

Table 9. List of powder properties determined in literature studies.

Generic property	Specific properties					
Morphology	Aspect ratio	Circularity	Sphericity	Symmetry		
Microstructure	Phases	Crystal structures				
Particle size distribution (PSD)	Full PSD	D_{10}	D_{50}	D_{80}	D_{85}	D_{90}
Interstitial element content	O content	N content	C content			
Elemental composition	Bulk composition		Surface composition			
Density (ρ)	ρ_{app}	ρ_{tap}	ρ_{true}	Packing at ρ_{app}		
Porosity						
Hardness						
Roughness						
Flowability	Hall flow rate Avalanche angle Break energy		Hausner Ratio Avalanche energy Rest angle	Carr Index Dynamic density Angle of repose		
Rheological performance[a]	BFE	SI	FRI			
	SE	CBD	CPS/CI			
	AIF	MPS	FF			
	WFA	UYS				
	Aeration Ratio/energy	Pressure drop				
	Permeability vs. applied normal stress	Bulk density				
	Shear stress vs. applied normal stress					
	Unconfined yield strength	Specific volume				
	Unconfined failure stress vs. major principal consolidating stress					
Thermal properties	Thermal conductivity		Thermographic analysis			
	Differential scanning calorimetry					
Magnetic properties	Magnetic moment	Coercivity	Susceptibility			

[a]BFE: basic flow energy; SI: stability index; FRI: flow rate index; SE: specific energy; CBD: conditioned bulk density; CPS/CI: compressibility/compressibility index; AIF: angle of internal friction; MPS: major principal stress; FF: flow friction; WFA: wall friction angle; UYS: unconfined yield strength.

terms was used, such as "times of reuse operations" [76], "repetitions of printing cycles" [90], "reuse times" [77], "recycled for… times" [80], "number of reuses" [105], "batch number" [97], "reused… times" [98], "build cycles ~reuse times" [82], "average usage time (AUT)" [81], "build number" [83] [86], "iteration…" [99], "number used" [94], "…printing jobs" [93], "reuse time" [95], and "print-

ing cycles" [100] [102]. In some studies, the number of cycles was not stated [75] [104].

Sixth, from the fourth- and fifth-mentioned issues above, it is clear that there is need for a consensus to be reached on definitions of "reuse" and "reuse cycle". After that, a recommendation should be made as to the minimum number of reuse cycles that should be used in studies on the influence of powder reuse on powder properties.

Seventh, there is a limited number of replication studies on the influence of powder reuse on powder properties (even in the case of Ti-6Al-4V alloy powder, which has attracted the most attention). One consequence of this shortcoming, coupled with the fourth- and fifth-mentioned issues stated above, is that, for a given alloy, it is very challenging to perform inter-study comparisons and, hence, to draw, isolate, and discuss consistent trends that may serve as the basis for improvements in the additive manufacturing of parts from the alloy.

Eighth, there is inconsistency on how the terms, "flowability" and "flowability rate" are used. It is recommended that "flowability rate" be used but with it defined as the inverse of the result obtained in a Hall test, as was done by Kroeger *et al.* [30]. In other words, present the result for flowability rate in the unit of 50 g/s or, simply, g/s.

Ninth, even though, in many studies, a sizeable number of properties of the powder particles were determined, there is very limited attempt in using these results to develop a methodology to guide powder selection. In fact, when such studies were conducted, the same approach was used [72] [87]. Brika *et al.* [72] presented such a methodology, culminating in the presentation of an "additive manufacturing suitability figure of merit (AMS)" applicable to an LB-PBF process, based on the arithmetic mean of the values of 7 flowability properties of a fresh powder (the closer AMS for a reused powder is that for a fresh powder, the more suitable the reused powder is for use in a laser powder bed fusion AM process). Similarly, Shangbag *et al.* [87] computed the arithmetic mean of 13 properties of fresh and reused powders and designated it an "electron beam powder bed fusion (EB-PBF) suitability factor (ESF)", with the lower the factor, the more suitable is the powder for use in an EB-PBF process. Two shortcomings of this approach are highlighted. First, equal weighting factors were assigned to each of the properties, and, second, well-established material selection methodologies, such as the Desirability Method [108], the VlseKriterijumska Optimazicija I Kompromisno Resenjein in Serbian (VIKOR) method [109], and the weighted aggregate sum product assessment (WASPAS) method [110], were not used. One of the many attractive features of each of these methodologies is that a distinction is made between properties that need to be maximized (in the case of powders, an example is circularity of the particle) and those that need to be minimized (in the case of powders, examples are powder SE, flow rate index, and repose angle) [111]).

Tenth, a few studies have been reported involving so-called "composite

powder feedstocks". Such a feedstock is defined herein as one in which a starting powder is modified by mechanical alloying (ball milling) with either an additive (for example, 316L stainless powder ball milled with 1 or 2 wt./wt% Y_2O_3 [112] or 1 wt./wt% CrN [113]) or deposition or coating of an additive on its surface (for example, 0.3 wt./wt% nano-sized Y_2O_3 deposited on the surface of a ferritic stainless steel powder [114]). In these reports, very few properties of the composite powder have been presented and there are no comparisons between those properties and those of the starting powder counterpart. Additional work in this area should be on developing other methods of obtaining composite powder feedstocks.

Eleventh, well-designed proof-of-concept studies should be conducted. One such study should compare powder produced using an established method (such as Ar gas atomization) versus powder produced using an emerging method (see Section 2) versus a composite powder feedstock, for a specified alloy. The comparison should include determination of powder properties (in particular, pore properties) as well as detailed characterization of the performance of a powder during part building using a specified powder-based MAM technology (for example, determination of melt pool geometry and spatter pattern if an LB-PBF method is used) as well as determination of a large assortment of properties of the built parts. These properties should include fatigue life under multiaxial loading conditions and spectrum loading conditions (using specimens that contain flaws, such as notches [115]), fatigue crack propagation rate [116], and corrosion performance (using a test medium that is appropriate for the anticipated service use of the built parts, such as phosphate buffered saline solution, at 37˚C, for alloys to be used to fabricate total joint replacements [117] [118]).

Twelfth, either limited or no attention has been paid to a number of issues. As such, there are many areas for future research. Example issues are 1) development of novel environmentally-friendly and low energy-intensive powder production methods [23]; 2) development of powder production methods that will yield powder particles that do not contain satellite particles; 3) development of international materials testing standards for determining rheological properties of powder (similar to ASTM 3049 [119]) and, as an adjunct to this effort, establishment of acceptable values of the properties (as has been done with O content, with the maximum allowable content being and 0.3 wt./wt% (per ASTM B988 [120]) and 0.2 wt./wt% (per ASTM F-3001 [121]) for Grade 5 and ELI Ti-6Al-4V alloys, respectively); 4) utilization of machine learning/artificial intelligence/deep learning methods to accomplish two purposes. The first would be determination of the key process variables, for a given powder production method. The second would be establishment of the influence of this collection of process variables on a large and varied assortment of powder properties, which would culminate in the optimization of these variables [122] [123]; 5) determination of influence of conditions under which a powder is stored prior to its use to build parts (notably, ambient temperature and relative humidity in the storage facility) on powder properties [124]; 6) development of novel methods of separation/fractionation

of as-received powder into a PSD that is suitable for a given powder-based MAM process, such as 20 - 63 μm-sized particles for LB-PBF of light metals [125]; 7) development of methods for improving flowability of a powder without adversely affecting any of its other properties, notably, PSD (and, hence, D_{50}) [126]; and 8) methods for producing high-quality powders of new/emerging metallic materials, such as multi-principal element alloys/complex concentrating alloys/high-entropy alloys (for example, FeCoNiCrAlCu [127]), Al crossover alloys (for example, AlMg4.7Zn3.6Cu0.6 [128]), ferritic oxide-dispersion-strengthened alloys that are strengthened by a yttrium-based nano-sized oxide (for example, Fe-10Al-4Cr-4Y_2O_3 [129]), and low-modulus β-Ti-based alloys (for example, Ti-38Nb-5Zr-2Ta-2Sn [130]), for use in powder-based MAM technologies.

8. Summary

The following are the main points made in the present review:

1) Methods of production of metal powders for use in powder-based MAM technologies are being expanded with the introduction of many emerging ones, such as plasma and gas hybrid atomization (PGHA), wire induction gas atomization, hydrogen-assisted magnesiothermic reduction, and a granulation-sintering-deoxygenation process. Extensive characterizations of metal powders produced from both established methods (such as argon gas atomization and water atomization) as well as emerging methods have been carried out. Powder properties determined include particle size distribution (PSD), phase composition, flowability, repose angle, and Carr Index. With each of the emerging methods, spherical powder was obtained.

2) In cases where powder produced using an established method is not spherical or very close to spherical, post-treatment methods have been presented for spheroidizing these powders. Two examples are a radiofrequency inductively coupled plasma process and ball milling.

3) Only a few studies have been conducted on the influence of process variables, for a given established powder production method, on powder properties. In one of these studies, it was found that, for AISI 316L austenitic stainless steel, the PSD (based on analysis of volume of particles) and flowability of powder produced using argon gas atomization were comparable to those of powder produced using nitrogen gas atomization but apparent density was lower and avalanche angle was greater for the powder produced using nitrogen gas. In another study, this one involving PREP-produced Ti-6Al-4V powder, median particle size decreased with the increase of electrode diameter, at a given electrode rotation speed.

4) Many of the studies on the influence of powder production method on powder properties have been on Ti-6Al-4V alloy powder and compared powders produced using GA, PREP, EIGA, and PA. One consistent trend is that compared to GA-produced powder, PA-produced powder had greater sphericity but comparable aspect ratio and PSD.

5) There is a sizeable volume of literature on the influence of powder reuse on a large assortment of properties of Ti-6Al-4V, Ni-based alloys (Inconel 718 and AT1718), stainless steels (316L, 304, and 17-4), and Al-based alloys (AlSi10Mg and Scalmaloy). However, because of variability in terms of number of studies (for a given alloy), powders studied, and powder properties determined, the only consistent trend is that for Ti-6Al-4V, Ni-based alloys, and stainless steels, powder reuse leads to marked increase in O content of the powder.

6) The literature on the aspects of the powder covered in the present review has many shortcomings and gaps, suggesting areas for future work. Examples of these areas are for one metal powder produced using one method, determination of a large and varied collection of powder properties as a function of powder reuse cycle (up to at least 50 cycles); for one metal powder, determination of a large and varied collection of properties when the production method is established (such as argon gas atomization) versus when it is an emerging method (such as PGHA); application of machine learning/artificial intelligence/deep technique method to determine the optimized values of all the key process parameters for a given combination of metal powder and powder production method; and development of methods of production of powders of new/emerging metallic materials, such as crossover Al alloys and low-modulus β-Ti alloys, for possible use in MAM technologies.

Acknowledgements

The author thanks Mr. Faridreza Attarzadeh, Department of Mechanical Engineering, The University of Memphis, for excellent editorial assistance (formatting the list of references, formatting the tables, and production of high-resolution figures).

Conflicts of Interest

The author declares no conflicts of interest regarding the publication of this paper.

References

[1] Grillo, G., Moridi, A., Stewart, E.J., Wakai, A., Assadi, H., Gartner, F., Guagliano, M., Klassen, T. and Dao, M. (2020) Solid-State Additive Manufacturing of Porous Ti-6Al-4V by Supersonic Impact. *Applied Materials Today*, **21**, Article ID: 100865. https://doi.org/10.1016/j.apmt.2020.100865

[2] Sadaf, M., Bragaglia, M. and Nanni, F. (2021) A Simple Route for Additive Manufacturing of 316L Stainless Steel via Fused Filament Fabrication. *Journal of Manufacturing Processes*, **67**, 141-150. https://doi.org/10.1016/j.jmapro.2021.04.055

[3] Fu, R., Tang, S., Lu, J., Cui, Y., Li, Z., Zhang, H., Xu, T., Chen, Z. and Liu, C. (2021) Hot-Wire Arc Additive Manufacturing of Aluminum Alloy with Reduced Porosity and High Deposition Rate. *Materials & Design*, **199**, Article ID: 109370. https://doi.org/10.1016/j.matdes.2020.109370

[4] Rodrigues, T.A., Duarte, V.R., Miranda, R.M., Santos, T.G. and Oliveira, J.P. (2021) Ultracold-Wire and Arc Additive Manufacturing (UC-WAAM). *Journal of Mate-*

rials Processing Technology, **296**, Article ID: 117196.
https://doi.org/10.1016/j.jmatprotec.2021.117196

[5] Abdulhameed, O., Al-Ahmari, A., Ameen, W. and Mian, S.H. (2019) Additive Manufacturing: Challenges, Trends, and Applications. *Advances in Mechanical Engineering*, **11**, 1-27. https://doi.org/10.1177/1687814018822880

[6] Jang, T.S., Kim, D.E., Han, G., Yoon, C.B. and Jung, H. (2020) Powder Based Additive Manufacturing for Biomedical Application of Titanium and Its Alloys: A Review. *Biomedical Engineering Letters*, **10**, 505-516.
https://doi.org/10.1007/s13534-020-00177-2

[7] Aversa, A., Saboori, A., Marchese, G., Iuliano, L., Lombardi, M. and Fino, P. (2021) Recent Progress in Beam-Based Metal Additive Manufacturing from a Materials Perspective: A Review of Patents. *Journal of Materials Engineering and Performance*, **30**, 8689-8699. https://doi.org/10.1007/s11665-021-06273-3

[8] Blakey-Milner, B., Gradl, P., Snedden, G., Brooks, M., Pitot, J., Lopez, E., Leary, M., Berto, F. and du Plessis, A. (2021) Metal Additive Manufacturing in Aerospace: A Review. *Materials & Design*, **209**, Article ID: 110008.
https://doi.org/10.1016/j.matdes.2021.110008

[9] Kladovasilakis, N., Charalampous, P., Kostavelis, I., Tzetzis, D. and Tzovaras, D. (2021) Impact of Metal Additive Manufacturing Parameters on the Powder Bed Fusion and Direct Energy Deposition Processes: A Comprehensive Review. *Progress in Additive Manufacturing*, **6**, 349-365. https://doi.org/10.1007/s40964-021-00180-8

[10] Kumar, S.P., Elangovan, S., Mohanraj, R. and Ramakrishna, J.R. (2021) Review on the Evolution and Technology of State-of-the-Art Metal Additive Manufacturing Processes. *Materials Today*: *Proceedings*, **46**, 7907-7920.
https://doi.org/10.1016/j.matpr.2021.02.567

[11] Popov, V.V., Grilli, M.L., Koptyug, A., Jaworska, L., Katz-Demyanetz, A., Klobčar, D., Balos, S., Postolnyi, B.O. and Goel, S. (2021) Powder Bed Fusion Additive Manufacturing Using Critical Raw Materials: A Review. *Materials*, **14**, 909.
https://doi.org/10.3390/ma14040909

[12] Svetlizky, D., Das, M., Zheng, B., Vyatskikh, A.L., Bose, S., Bandyopadhyay, A., Schoenung, J.M., Lavernia, E.J. and Eliaz, N. (2021) Directed Energy Deposition (DED) Additive Manufacturing: Physical Characteristics, Defects, Challenges and Applications. *Materials Today*, **49**, 271-295.
https://doi.org/10.1016/j.mattod.2021.03.020

[13] Tan, C., Weng, F., Sui, S., Chew, Y. and Bi, G. (2021) Progress and Perspectives in Laser Additive Manufacturing of Key Aeroengine Materials. *International Journal of Machine Tools and Manufacture*, **170**, Article ID: 103804.
https://doi.org/10.1016/j.ijmachtools.2021.103804

[14] Vafadar, A., Guzzomi, F., Rassau, A. and Hayward, K. (2021) Advances in Metal Additive Manufacturing: A Review of Common Processes, Industrial Applications, and Current Challenges. *Applied Sciences*, **11**, 1213.
https://doi.org/10.3390/app11031213

[15] Vignesh, M., Ranjith Kumar, G., Sathishkumar, M., Manikandan, M., Rajyalakshmi, G., Ramanujam, R. and Arivazhagan, N. (2021) Development of Biomedical Implants through Additive Manufacturing: A Review. *Journal of Materials Engineering and Performance*, **30**, 4735-4744. https://doi.org/10.1007/s11665-021-05578-7

[16] Jelis, E., Clemente, M., Hespos, M., Groeschler, S., Golden, E. and Carpenter, R. (2021) Round Robin Study Evaluating Consistency of 4340 Steel Specimens Manufactured by Different Laser Powder Bed Fusion Machines. *Journal of Materials En-*

gineering and Performance, **30**, 6832-6843.
https://doi.org/10.1007/s11665-021-06020-8

[17] Prater, T. (2017) Database Development for Additive Manufacturing. *Progress in Additive Manufacturing*, **2**, 11-18. https://doi.org/10.1007/s40964-017-0016-0

[18] Magnien, J., Cosemans, P., Nutal, N. and Kairet, T. (2020) Current Surface Issues in Additive Manufacturing. *Plasma Processes and Polymers*, **17**, Article ID: 1900154. https://doi.org/10.1002/ppap.201900154

[19] Kandukuri, S., Günay, E.E., Al-Araidah, O. and Okudan Kremer, G.E. (2021) Inventive Solutions for Remanufacturing Using Additive Manufacturing: ETRIZ. *Journal of Cleaner Production*, **305**, Article ID: 126992. https://doi.org/10.1016/j.jclepro.2021.126992

[20] Carpenter, K. and Tabei, A. (2020) On Residual Stress Development, Prevention, and Compensation in Metal Additive Manufacturing. *Materials*, **13**, 255. https://doi.org/10.3390/ma13020255

[21] Kelly, C.N., Wang, T., Crowley, J., Wills, D., Pelletier, M.H., Westrick, E.R., Adams, S.B., Gall, K. and Walsh, W.R. (2021) High-Strength, Porous Additively Manufactured Implants with Optimized Mechanical Osseointegration. *Biomaterials*, **279**, Article ID: 121206. https://doi.org/10.1016/j.biomaterials.2021.121206

[22] Gao, C., Wolff, S. and Wang, S. (2021) Eco-Friendly Additive Manufacturing of Metals: Energy Efficiency and Life Cycle Analysis. *Journal of Manufacturing Systems*, **60**, 459-472. https://doi.org/10.1016/j.jmsy.2021.06.011

[23] Liao, J. and Cooper, D.R. (2021) The Environmental Impacts of Metal Powder Bed Additive Manufacturing. *Journal of Manufacturing Science and Engineering*, **143**, Article ID: 03081. https://doi.org/10.1115/1.4048435

[24] Lv, J., Peng, T., Zhang, Y. and Wang, Y. (2020) A Novel Method to Forecast Energy Consumption of Selective Laser Melting Processes. *International Journal of Production Research*, **59**, 2375-2391. https://doi.org/10.1080/00207543.2020.1733126

[25] Sun, C. and Shang, G. (2021) Application of Metal Additive Manufacturing. *World Journal of Engineering and Technology*, **9**, 194-202. https://doi.org/10.4236/wjet.2021.91014

[26] Olakanmi, E.O., Cochrane, R.F. and Dalgarno, K.W. (2015) A Review on Selective Laser Sintering/Melting (SLS/SLM) of Aluminium Alloy Powders: Processing, Microstructure, and Properties. *Progress in Materials Science*, **74**, 401-477. https://doi.org/10.1016/j.pmatsci.2015.03.002

[27] Spierings, A.B., Voegtlin, M., Bauer, T. and Wegener, K. (2016) Powder Flowability Characterisation Methodology for Powder-Bed-Based Metal Additive Manufacturing. *Progress in Additive Manufacturing*, **1**, 9-20. https://doi.org/10.1007/s40964-015-0001-4

[28] Sutton, A.T., Kriewall, C.S., Leu, M.C. and Newkirk, J.W. (2016) Powder Characterisation Techniques and Effects of Powder Characteristics on Part Properties in Powder-Bed Fusion Processes. *Virtual and Physical Prototyping*, **12**, 3-29. https://doi.org/10.1080/17452759.2016.1250605

[29] Vock, S., Klöden, B., Kirchner, A., Weißgärber, T. and Kieback, B. (2019) Powders for Powder Bed Fusion: A Review. *Progress in Additive Manufacturing*, **4**, 383-397. https://doi.org/10.1007/s40964-019-00078-6

[30] Kroeger, J., Poirié, T., Moghimian, P., Marion, F. and Larouche, F. (2021) Flow Rate Ranges for Spherical Metallic Powders for Additive Manufacturing. *Progress in Additive Manufacturing*, **7**, 411-418. https://doi.org/10.1007/s40964-021-00238-7

[31] Antony, L.V.M. and Reddy, R.G. (2003) Processes for Production of High-Purity

Metal Powders. *JOM*, **55**, 14-18. https://doi.org/10.1007/s11837-003-0153-4

[32] McCracken, C.G., Motchenbacher, C. and Barbis, D.P. (2010) Review of Titanium-Powder-Production Methods. *International Journal of Powder Metallurgy*, **46**, 19-26.

[33] Dawes, J., Bowerman, R. and Trepleton, R. (2015) Introduction to the Additive Manufacturing Powder Metallurgy Supply Chain. *Johnson Matthey Technology Review*, **59**, 243-256. https://doi.org/10.1595/205651315X688686

[34] Dietrich, S., Wunderer, M., Huissel, A. and Zaeh, M.F. (2016) A New Approach for a Flexible Powder Production for Additive Manufacturing. *Procedia Manufacturing*, **6**, 88-95. https://doi.org/10.1016/j.promfg.2016.11.012

[35] Mellor, I. and Doughty, G. (2016) Novel and Emerging Routes for Titanium Powder Production—An Overview. *Key Engineering Materials*, **704**, 271-281. https://doi.org/10.4028/www.scientific.net/KEM.704.271

[36] Sun, P., Fang, Z.Z., Zhang, Y. and Xia, Y. (2017) Review of the Methods for Production of Spherical Ti and Ti Alloy Powder. *JOM*, **69**, 1853-1860. https://doi.org/10.1007/s11837-017-2513-5

[37] Mostafaei, A., Hilla, C., Stevens, E.L., Nandwana, P., Elliott, A.M. and Chmielus, M. (2018) Comparison of Characterization Methods for Differently Atomized Nickel-Based Alloy 625 Powders. *Powder Technology*, **333**, 180-192. https://doi.org/10.1016/j.powtec.2018.04.014

[38] Kassym, K. and Perveen, A. (2020) Atomization Processes of Metal Powders for 3D Printing. *Materials Today*: *Proceedings*, **26**, 1727-1733. https://doi.org/10.1016/j.matpr.2020.02.364

[39] Garboczi, E.J. and Hrabe, N. (2020) Particle Shape and Size Analysis for Metal Powders Used for Additive Manufacturing: Technique Description and Application to Two Gas-Atomized and Plasma-Atomized Ti64 Powders. *Additive Manufacturing*, **31**, Article ID: 100965. https://doi.org/10.1016/j.addma.2019.100965

[40] Mitterlehner, M., Danninger, H., Gierl-Mayer, C., Gschiel, H., Martinez, C., Tomisser, M., Schatz, M., Senck, S., Auer, J. and Benigni, C. (2021) Comparative Evaluation of Characterization Methods for Powders Used in Additive Manufacturing, *Journal of Materials Engineering and Performance*, **30**, 7019-7034. https://doi.org/10.1007/s11665-021-06113-4

[41] Moghimian, P., Poirié, T., Habibnejad-Korayem, M., Zavala, J.A., Kroeger, J., Marion, F. and Larouche, F. (2021) Metal Powders in Additive Manufacturing: A Review on Reusability and Recyclability of Common Titanium, Nickel and Aluminum Alloys. *Additive Manufacturing*, **43**, Article ID: 102017. https://doi.org/10.1016/j.addma.2021.102017

[42] Slotwinski, J.A., Garboczi, E.J., Stutzman, P.E., Ferraris, C.F., Watson, S.S. and Peltz, M.A. (2014) Characterization of Metal Powders Used for Additive Manufacturing. *Journal of Research of the National Institute of Standards and Technology*, **119**, 460. https://doi.org/10.6028/jres.119.018

[43] Irrinki, H., Harper, T., Badwe, S., Stitzel, J., Gulsoy, O., Gupta, G. and Atre, S.V. (2018) Effects of Powder Characteristics and Processing Conditions on the Corrosion Performance of 17-4 PH Stainless Steel Fabricated by Laser-Powder Bed Fusion. *Progress in Additive Manufacturing*, **3**, 39-49. https://doi.org/10.1007/s40964-018-0048-0

[44] Santecchia, E., Spigarelli, S. and Cabibbo, M. (2020) Material Reuse in Laser Powder Bed Fusion: Side Effects of the Laser—Metal Powder Interaction. *Metals*, **10**, 341. https://doi.org/10.3390/met10030341

[45] Kang, I.J., Park, H.J., Cho, C.H., Kim, J.H., Kim, H.K., Kim, I.K. and Park, S.J. (2021) Development of a Plasma and Gas Hybrid Atomization System for the Production of Metal Powder Materials. *Journal of the Korean Physical Society*, **79**, 1141-1150. https://doi.org/10.1007/s40042-021-00341-6

[46] Zheng, M., Zhang, S., Hu, Q., Xu, J., Mao, W., Lu, L., He, H., Liu, Y. and Zhao, W. (2018) A Novel Crucible-Less Inert Gas Atomisation Method of Producing Titanium Powder for Additive Manufacturing. *Powder Metallurgy*, **62**, 15-21. https://doi.org/10.1080/00325899.2018.1540525

[47] Canakci, A. and Varol, T. (2015) A Novel Method for the Production of Metal Powders without Conventional Atomization Process. *Journal of Cleaner Production*, **99**, 312-319. https://doi.org/10.1016/j.jclepro.2015.02.090

[48] Fullenwider, B., Kiani, P., Schoenung, J.M. and Ma, K. (2019) From Recycled Machining Waste to Useful Powders for Metal Additive Manufacturing. In: Azizi, A. and Yazdi, P.G., Eds., *Computer-Based Analysis of the Stochastic Stability of Mechanical Structures Driven by White and Colored Noise*, Springer, Berlin, 3-7. https://doi.org/10.1007/978-3-030-10386-6_1

[49] Xia, Y., Fang, Z.Z., Zhang, Y., Lefler, H., Zhang, T., Sun, P. and Huang, Z. (2017) Hydrogen Assisted Magnesiothermic Reduction (HAMR) of Commercial TiO_2 to Produce Titanium Powder with Controlled Morphology and Particle Size. *Materials Transactions*, **58**, 355-360. https://doi.org/10.2320/matertrans.MK201628

[50] ASTM B299/B299M-18 (2018) Standard Specification for Titanium Sponge. ASTM International, West Conshohocken.

[51] Doblin, C., Chryss, A. and Monch, A. (2012) Titanium Powder from the TiRO^{TM} Process. *Key Engineering Materials*, **520**, 95-100. https://doi.org/10.4028/www.scientific.net/KEM.520.95

[52] Doblin, C., Freeman, D. and Richards, M. (2013) The TiRO^{TM} Process for the Continuous Direct Production of Titanium Powder. *Key Engineering Materials*, **551**, 37-43. https://doi.org/10.4028/www.scientific.net/KEM.551.37

[53] Ahmadi, E. and Suzuki, R.O. (2020) An Innovative Process for Production of Ti Metal Powder via TiSx from TiN. *Metallurgical and Materials Transactions B: Process Metallurgy and Materials Processing Science*, **51**, 140-148. https://doi.org/10.1007/s11663-019-01730-w

[54] Sun, P., Fang, Z.Z., Xia, Y., Zhang, Y. and Zhou, C. (2016) A Novel Method for Production of Spherical Ti-6Al-4V Powder for Additive Manufacturing. *Powder Technology*, **301**, 331-335. https://doi.org/10.1016/j.powtec.2016.06.022

[55] Bao, Q., Yang, Y., Wen, X., Guo, L. and Guo, Z. (2021) The Preparation of Spherical Metal Powders Using the High-Temperature Remelting Spheroidization Technology. *Materials & Design*, **199**, Article ID: 109382. https://doi.org/10.1016/j.matdes.2020.109382

[56] Simonelli, M., Aboulkhair, N.T., Cohen, P., Murray, J.W., Clare, A.T., Tuck, C. and Hague, R.J.M. (2018) A Comparison of Ti-6Al-4V *In-Situ* Alloying in Selective Laser Melting Using Simply-Mixed and Satellited Powder Blend Feedstocks. *Materials Characterization*, **143**, 118-126. https://doi.org/10.1016/j.matchar.2018.05.039

[57] Vert, R., Pontone, R., Dolbec, R., Dionne, L. and Boulos, M.I. (2016) Induction Plasma Technology Applied to Powder Manufacturing: Example of Titanium-Based Materials. *Key Engineering Materials*, **704**, 282-286. https://doi.org/10.4028/www.scientific.net/KEM.704.282

[58] Liu, B., He, G., Liu, Y., Yue, M. and Lian, L. (2021) High-Quality Spherical Zirconium Alloy Powders Prepared by Thermal Plasma Treatment for Additive Manu-

facturing. *Materials Letters*, **288**, Article ID: 129360. https://doi.org/10.1016/j.matlet.2021.129360

[59] Qin, Q., Yang, F., Shi, T., Guo, Z., Sun, H., Li, P., Lu, X., Chen, C., Hao, J. and Cao, P. (2019) Spheroidization of Tantalum Powder by Radio Frequency Inductively Coupled Plasma Processing. *Advanced Powder Technology*, **30**, 1709-1714. https://doi.org/10.1016/j.apt.2019.05.022

[60] Ding, W., Chen, G., Qin, M., He, Y. and Qu, X. (2019) Low-Cost Ti Powders for Additive Manufacturing Treated by Fluidized Bed. *Powder Technology*, **350**, 117-122. https://doi.org/10.1016/j.powtec.2019.03.042

[61] Cordova, L., Bor, T., de Smit, M., Campos, M. and Tinga, T. (2020) Measuring the Spreadability of Pre-Treated and Moisturized Powders for Laser Powder Bed Fusion. *Additive Manufacturing*, **32**, Article ID: 101082. https://doi.org/10.1016/j.addma.2020.101082

[62] Kellogg, F., Kudzal, A., Mock, C., Taggart-Scarff, J., Rogers, R. and McWilliams, B. (2020) Feasibility of Cryomilled 17-4 Stainless Steel Powder as Feedstock for Additive Manufacturing. https://apps.dtic.mil/sti/citations/AD1100837

[63] Ansell, T.Y., Hanneman, T., Gonzalez-Perez, A., Park, C. and Nieto, A. (2021) Effect of High Energy Ball Milling on Spherical Metallic Powder Particulates for Additive Manufacturing. *Particulate Science and Technology*, **39**, 981-989. https://doi.org/10.1080/02726351.2021.1876192

[64] Dong, Y.P., Li, Y.L., Zhou, S.Y., Zhou, Y.H., Dargusch, M.S., Peng, H.X. and Yan, M. (2021) Cost-Affordable Ti-6Al-4V for Additive Manufacturing: Powder Modification, Compositional Modulation and Laser *In-Situ* Alloying. *Additive Manufacturing*, **37**, Article ID: 101699. https://doi.org/10.1016/j.addma.2020.101699

[65] Wang, D.W., Zhou, Y.H., Yao, X.Y., Dong, Y.P., Feng, S.H., Liu, Z.Y., Wang, H. and Yan, M. (2022) Inheritance of Microstructure and Mechanical Properties in Laser Powder Bed Fusion Additive Manufacturing: A Feedstock Perspective. *Materials Science and Engineering*: *A*, **832**, Article ID: 142311. https://doi.org/10.1016/j.msea.2021.142311

[66] Gao, M.Z., Ludwig, B. and Palmer, T.A. (2021) Impact of Atomization Gas on Characteristics of Austenitic Stainless Steel Powder Feedstocks for Additive Manufacturing. *Powder Technology*, **383**, 30-42. https://doi.org/10.1016/j.powtec.2020.12.005

[67] Cui, Y., Zhao, Y., Numata, H., Yamanaka, K., Bian, H., Aoyagi, K. and Chiba, A. (2021) Effects of Process Parameters and Cooling Gas on Powder Formation during the Plasma Rotating Electrode Process. *Powder Technology*, **393**, 301-311. https://doi.org/10.1016/j.powtec.2021.07.062

[68] Karlsson, J., Snis, A., Engqvist, H. and Lausmaa, J. (2013) Characterization and Comparison of Materials Produced by Electron Beam Melting (EBM) of Two Different Ti-6Al-4V Powder Fractions. *Journal of Materials Processing Technology*, **213**, 2109-2118. https://doi.org/10.1016/j.jmatprotec.2013.06.010

[69] Guo, R.P., Xu, L., Zong, B.Y.P. and Yang, R. (2017) Characterization of Prealloyed Ti-6Al-4V Powders from EIGA and PREP Process and Mechanical Properties of Hiped Powder Compacts. *Acta Metallurgica Sinica* (*English Letters*), **30**, 735-744. https://doi.org/10.1007/s40195-017-0540-4

[70] Chen, G., Zhao, S.Y., Tan, P., Wang, J., Xiang, C.S. and Tang, H.P. (2018) A Comparative Study of Ti-6Al-4V Powders for Additive Manufacturing by Gas Atomization, Plasma Rotating Electrode Process and Plasma Atomization. *Powder Technology*, **333**, 38-46. https://doi.org/10.1016/j.powtec.2018.04.013

[71] Sun, Y., Aindow, M. and Hebert, R.J. (2018) Comparison of Virgin Ti-6Al-4V Powders for Additive Manufacturing. *Additive Manufacturing*, **21**, 544-555. https://doi.org/10.1016/j.addma.2018.02.011

[72] Brika, S.E., Letenneur, M., Dion, C.A. and Brailovski, V. (2020) Influence of Particle Morphology and Size Distribution on the Powder Flowability and Laser Powder Bed Fusion Manufacturability of Ti-6Al-4V Alloy. *Additive Manufacturing*, **31**, Article ID: 100929. https://doi.org/10.1016/j.addma.2019.100929

[73] Guzmán, J., de Moura Nobre, R., Rodrigues Júnior, D.L., de Morais, W.A., Nunes, E.R., Bayerlein, D.L., Falcão, R.B., Sallica-Leva, E., Oliveira, H.R., Chastinet, V.L. and Landgraf, F.J.G. (2021) Comparing Spherical and Irregularly Shaped Powders in Laser Powder Bed Fusion of Nb47Ti Alloy. *Journal of Materials Engineering and Performance*, **30**, 6557-6567. https://doi.org/10.1007/s11665-021-05916-9

[74] Seyda, V., Kaufmann, N. and Emmelmann, C. (2012) Investigation of Aging Processes of Ti-6Al-4 V Powder Material in Laser Melting. *Physics Procedia*, **39**, 425-431. https://doi.org/10.1016/j.phpro.2012.10.057

[75] Strondl, A., Lyckfeldt, O., Brodin, H. and Ackelid, U. (2015) Characterization and Control of Powder Properties for Additive Manufacturing. *JOM*, **67**, 549-554. https://doi.org/10.1007/s11837-015-1304-0

[76] Tang, H.P., Qian, M., Liu, N., Zhang, X.Z., Yang, G.Y. and Wang, J. (2015) Effect of Powder Reuse Times on Additive Manufacturing of Ti-6Al-4V by Selective Electron Beam Melting. *JOM*, **67**, 555-563. https://doi.org/10.1007/s11837-015-1300-4

[77] Wei, C., Ma, X., Yang, X., Zhou, M., Wang, C., Zheng, Y., Zhang, W. and Li, Z. (2018) Microstructural and Property Evolution of Ti6Al4V Powders with the Number of Usage in Additive Manufacturing by Electron Beam Melting. *Materials Letters*, **221**, 111-114. https://doi.org/10.1016/j.matlet.2018.03.124

[78] Popov, V.V., Katz-Demyanetz, A., Garkun, A. and Bamberger, M. (2018) The Effect of Powder Recycling on the Mechanical Properties and Microstructure of Electron Beam Melted Ti-6Al-4 V Specimens. *Additive Manufacturing*, **22**, 834-843. https://doi.org/10.1016/j.addma.2018.06.003

[79] Quintana, O.A., Alvarez, J., Mcmillan, R., Tong, W. and Tomonto, C. (2018) Effects of Reusing Ti-6Al-4V Powder in a Selective Laser Melting Additive System Operated in an Industrial Setting. *JOM*, **70**, 1863-1869. https://doi.org/10.1007/s11837-018-3011-0

[80] Carrion, P.E., Soltani-Tehrani, A., Phan, N. and Shamsaei, N. (2019) Powder Recycling Effects on the Tensile and Fatigue Behavior of Additively Manufactured Ti-6Al-4V Parts. *JOM*, **71**, 963-973. https://doi.org/10.1007/s11837-018-3248-7

[81] Denti, L., Sola, A., Defanti, S., Sciancalepore, C. and Bondioli, F. (2019) Effect of Powder Recycling in Laser-Based Powder Bed Fusion of Ti-6Al-4V. *Manufacturing Technology*, **19**, 190-196. https://doi.org/10.21062/ujep/268.2019/a/1213-2489/MT/19/2/190

[82] Cordova, L., Campos, M. and Tinga, T. (2019) Revealing the Effects of Powder Reuse for Selective Laser Melting by Powder Characterization. *JOM*, **71**, 1062-1072. https://doi.org/10.1007/s11837-018-3305-2

[83] Ghods, S., Schultz, E., Wisdom, C., Schur, R., Pahuja, R., Montelione, A., Arola, D. and Ramulu, M. (2020) Electron Beam Additive Manufacturing of Ti6Al4V: Evolution of Powder Morphology and Part Microstructure with Powder Reuse. *Materialia*, **9**, Article ID: 100631. https://doi.org/10.1016/j.mtla.2020.100631

[84] ASTM F2924-14 (2021) Standard Specification for Additive Manufacturing Titanium-6 Aluminum-4 Vanadium with Powder Bed Fusion. ASTM International,

West Conshohocken.

[85] Cao, Y., Delin, M., Kullenberg, F. and Nyborg, L. (2020). Surface Modification of Ti-6Al-4V Powder during Recycling in EBM Process. *Surface and Interface Analysis*, **52**, 1066-1070. https://doi.org/10.1002/sia.6847

[86] Chandrasekar, S., Coble, J.B., Yoder, S., Nandwana, P., Dehoff, R.R., Paquit, V.C. and Babu, S.S. (2020) Investigating the Effect of Metal Powder Recycling in Electron Beam Powder Bed Fusion Using Process Log Data. *Additive Manufacturing*, **32**, Article ID: 100994. https://doi.org/10.1016/j.addma.2019.100994

[87] Shanbhag, G. and Vlasea, M. (2021) Powder Reuse Cycles in Electron Beam Powder Bed Fusion—Variation of Powder Characteristics. *Materials*, **14**, 4602. https://doi.org/10.3390/ma14164602

[88] Ardila, L.C., Garciandia, F., González-Díaz, J.B., Álvarez, P., Echeverria, A., Petite, M.M., Deffley, R. and Ochoa, J. (2014) Effect of IN718 Recycled Powder Reuse on Properties of Parts Manufactured by Means of Selective Laser Melting. *Physics Procedia*, **56**, 99-107. https://doi.org/10.1016/j.phpro.2014.08.152

[89] Renderos, M., Girot, F., Lamikiz, A., Torregaray, A. and Saintier, N. (2016) Ni Based Powder Reconditioning and Reuse for LMD Process. *Physics Procedia*, **83**, 769-777. https://doi.org/10.1016/j.phpro.2016.08.079

[90] Nguyen, Q.B., Nai, M.L.S., Zhu, Z., Sun, C.N., Wei, J. and Zhou, W. (2017) Characteristics of Inconel Powders for Powder-Bed Additive Manufacturing. *Engineering*, **3**, 695-700. https://doi.org/10.1016/J.ENG.2017.05.012

[91] Kappes, B., Moorthy, S., Drake, D., Geerlings, H. and Stebner, A. (2018) Machine Learning to Optimize Additive Manufacturing Parameters for Laser Powder Bed Fusion of Inconel 718. In: Ott, E., *et al.*, Eds., *Proceedings of the 9th International Symposium on Superalloy 718 & Derivatives: Energy, Aerospace, and Industrial Applications*, The Minerals, Metals & Materials Series, Springer, Berlin, 595-610. https://doi.org/10.1007/978-3-319-89480-5_39

[92] Gruber, H., Henriksson, M., Hryha, E. and Nyborg, L. (2019) Effect of Powder Recycling in Electron Beam Melting on the Surface Chemistry of Alloy 718 Powder. *Metallurgical and Materials Transactions A: Physical Metallurgy and Materials Science*, **50**, 4410-4422. https://doi.org/10.1007/s11661-019-05333-7

[93] Paccou, E., Mokhtari, M., Keller, C., Nguejio, J., Lefebvre, W., Sauvage, X., Boileau, S., Babillot, P., Bernard, P. and Bauster, E. (2021) Investigations of Powder Reusing on Microstructure and Mechanical Properties of Inconel 718 Obtained by Additive Manufacturing. *Materials Science and Engineering A*, **828**, Article ID: 142113. https://doi.org/10.1016/j.msea.2021.142113

[94] Rock, C., Ledford, C., Garcia-Avila, M., West, H., Miller, V.M., Pankow, M., Dehoff, R. and Horn, T. (2021) The Influence of Powder Reuse on the Properties of Nickel Super Alloy ATI 718™ in Laser Powder Bed Fusion Additive Manufacturing. *Metallurgical and Materials Transactions B: Process Metallurgy and Materials Processing Science*, **52**, 676-688. https://doi.org/10.1007/s11663-020-02040-2

[95] Yi, F., Zhou, Q., Wang, C., Yan, Z. and Liu, B. (2021) Effect of Powder Reuse on Powder Characteristics and Properties of Inconel 718 Parts Produced by Selective Laser Melting. *Journal of Materials Research and Technology*, **13**, 524-533. https://doi.org/10.1016/j.jmrt.2021.04.091

[96] Zhang, J., Hu, B., Zhang, Y., Guo, X., Wu, L., Park, H.Y., Lee, J. and Jung, Y.G. (2018) Comparison of Virgin and Reused 15-5 PH Stainless Steel Powders for Laser Powder Bed Fusion Process. *Progress in Additive Manufacturing*, **3**, 11-14. https://doi.org/10.1007/s40964-018-0038-2

[97] Soltani-Tehrani, A., Pegues, J. and Shamsaei, N. (2020) Fatigue Behavior of Additively Manufactured 17-4PH Stainless Steel: The Effects of Part Location and Powder Re-Use. *Additive Manufacturing*, **36**, Article ID: 101398. https://doi.org/10.1016/j.addma.2020.101398

[98] Heiden, M.J., Deibler, L.A., Rodelas, J.M., Koepke, J.R., Tung, D.J., Saiz, D.J. and Jared, B.H. (2019) Evolution of 316L Stainless Steel Feedstock Due to Laser Powder Bed Fusion Process. *Additive Manufacturing*, **25**, 84-103. https://doi.org/10.1016/j.addma.2018.10.019

[99] Sutton, A.T., Kriewall, C.S., Karnati, S., Leu, M.C. and Newkirk, J.W. (2020) Characterization of AISI 304L Stainless Steel Powder Recycled in the Laser Powder-Bed Fusion Process. *Additive Manufacturing*, **32**, Article ID: 100981. https://doi.org/10.1016/j.addma.2019.100981

[100] Gorji, N.E., Saxena, P., Corfield, M., Clare, A., Rueff, J.P., Bogan, J., González, P.G.M., Snelgrove, M., Hughes, G., O'Connor, R., Raghavendra, R. and Brabazon, D. (2020) A New Method for Assessing the Recyclability of Powders within Powder Bed Fusion Process. *Materials Characterization*, **161**, Article ID: 110167. https://doi.org/10.1016/j.matchar.2020.110167

[101] Yusuf, S.M., Choo, E. and Gao, N. (2020) Comparison between Virgin and Recycled 316L SS and AlSi10Mg Powders Used for Laser Powder Bed Fusion Additive Manufacturing. *Metals*, **10**, 1625. https://doi.org/10.3390/met10121625

[102] Delacroix, T., Lomello, F., Schuster, F., Maskrot, H. and Garandet, J.-P. (2022). Influence of Powder Recycling on 316L Stainless Steel Feedstocks and Printed Parts in Laser Powder Bed Fusion. *Additive Manufacturing*, **50**, Article ID: 102553. https://doi.org/10.1016/j.addma.2021.102553

[103] Asgari, H., Baxter, C., Hosseinkhani, K. and Mohammadi, M. (2017) On Microstructure and Mechanical Properties of Additively Manufactured AlSi10Mg_200C Using Recycled Powder. *Materials Science and Engineering*: *A*, **707**, 148-158. https://doi.org/10.1016/j.msea.2017.09.041

[104] Maamoun, A.H., Elbestawi, M., Dosbaeva, G.K. and Veldhuis, S.C. (2018) Thermal Post-Processing of AlSi10Mg Parts Produced by Selective Laser Melting Using Recycled Powder. *Additive Manufacturing*, **21**, 234-247. https://doi.org/10.1016/j.addma.2018.03.014

[105] Del Re, F., Contaldi, V., Astarita, A., Palumbo, B., Squillace, A., Corrado, P. and Di Petta, P. (2018) Statistical Approach for Assessing the Effect of Powder Reuse on the Final Quality of AlSi10Mg Parts Produced by Laser Powder Bed Fusion Additive Manufacturing. *The International Journal of Advanced Manufacturing Technology*, **97**, 2231-2240. https://doi.org/10.1007/s00170-018-2090-y

[106] Raza, A., Fiegl, T., Hanif, I., MarkstrÖm, A., Franke, M., Körner, C. and Hryha, E. (2021) Degradation of AlSi10Mg Powder during Laser Based Powder Bed Fusion Processing. *Materials & Design*, **198**, Article ID: 109358. https://doi.org/10.1016/j.matdes.2020.109358

[107] ASTM Standard E1409-05 (2013) Standard Test Method for Determination of Oxygen and Nitrogen in Titanium and Titanium Alloys by the Inert Gas Fusion Technique. ASTM International, West Conshohocken.

[108] Karande, P., Gauri, S.K. and Chakraborty, S. (2013) Applications of Utility Concept and Desirability Function for Materials Selection. *Materials & Design*, **45**, 349-358. https://doi.org/10.1016/j.matdes.2012.08.067

[109] Opricovic, S. (1998) Multicriteria Optimization of Civil Engineering Systems. Ph.D. Dissertation, University of Belgrade, Serbia.

[110] Kumar, R., Dubey, R., Singh, S., Sunpreet, P.C., Nirsanametla, Y., Królczyk, G. and Chudy, R. (2021) Multiple-Criteria Decision-Making and Sensitivity Analysis for Selection of Materials for Knee Implant Femoral Component. *Materials*, **14**, 2084. https://doi.org/10.3390/ma14082084

[111] Mussatto, A., Groarke, R., O'Neill, A., Obeidi, M.A., Delaure, Y. and Brabazon, D. (2021) Influences of Powder Morphology and Spreading Parameters on the Powder Bed Topography Uniformity in Powder Bed Fusion Metal Additive Manufacturing. *Additive Manufacturing*, **38**, Article ID: 101807. https://doi.org/10.1016/j.addma.2020.101807

[112] Zhong, Y., Liu, L., Zou, J., Li, X., Cui, D. and Shen, Z. (2020) Oxide Dispersion Strengthened Stainless Steel 316L with Superior Strength and Ductility by Selective Laser Melting. *Journal Mateerials Science and Technology*, **42**, 97-105. https://doi.org/10.1016/j.jmst.2019.11.004

[113] Vukkum, V.B., Christudasjustus, J., Darwish, A.A., Storck, S.M. and Gupta, R.K. (2022) Enhanced Corrosion Resistance of Additively Manufactured Stainless Steel by Modification of Feedstock. *NPJ Materials Degradation*, **6**, 2. https://doi.org/10.1038/s41529-021-00215-z

[114] Wilms, M.B., Streubel, R., Fromel, F., Weisheit, A., Tenkamp, J., Walther, F., Barcikowski, S., Schleifenbaum, J.H. and Gokce, B. (2018) Laser Additive Manufacturing of Oxide Dispersion Steels Using Laser-Generated Nanoparticle-Metal Composite Powders. *Procedia CIRP*, **74**, 196-200. https://doi.org/10.1016/j.procir.2018.08.093

[115] Molaei, R. and Fatemi, A. (2021) Fatigue Performance of Additive Manufactured Metals under Variable Amplitude Service Loading Conditions Including Multiaxial Stresses and Notch Effects: Experiments and Modelling. *International Journal of Fatigue*, **145**, Article ID: 106002. https://doi.org/10.1016/j.ijfatigue.2020.106002

[116] Jones, R., Cizek, J., Kovarik, O., Ang, A. and Champagne, V. (2022) Observations on Comparable Aluminium Alloy Crack Growth Curves: Additively Manufactured Scalmalloy® as an Alternative to AA5754 and AA6061-T6 Alloys? *Additive Manufacturing Letters*, **2**, Article ID: 100026. https://doi.org/10.1016/j.addlet.2022.100026

[117] Leon, A., Levy, G.K., Ron, T., Shirizly, A. and Aghion, E. (2020) The Effect of Hot Isostatic Pressure on the Corrosion Performance of Ti-6Al-4 V Produced by an Electron-Beam Melting Additive Manufacturing Process. *Additive Manufacturing*, **33**, Article ID: 101039. https://doi.org/10.1016/j.addma.2020.101039

[118] Li, X., Li, D., Li, G. and Cai, Q. (2022) Microstructure, Mechanical Properties, Aging Behavior, and Corrosion Resistance of a Laser Powder Bed Fusion Fabricated Al-Zn-Mg-Cu-Ta Alloy. *Materials Science and Engineering*: *A*, **832**, Article ID: 142364. https://doi.org/10.1016/j.msea.2021.142364

[119] ASTM Standard F3049-14 (2021) Standard Guide for Characterizing Properties of Metal Powders Used for Additive Manufacturing Processes. ASTM International, West Conshohocken.

[120] ASTM Standard B988-18 (2018) Standard Specification for Powder Metallurgy (PM) Titanium and Titanium Alloy Structural Components. ASTM International, West Conshohocken.

[121] ASTM Standard F3001 (2021) Standard Specification for Additive Manufacturing Titanium-6 Aluminum-4 Vanadium ELI (Extra Low Interstitial) with Powder Bed Fusion. ASTM International, West Conshohocken. https://www.astm.org/f3001-14r21.html

[122] Sing, S.L., Kuo, C.N., Shih, C.T., Ho, C.C. and Chua, C.K. (2021) Perspectives of

Using Machine Learning in Laser Powder Bed Fusion for Metal Additive Manufacturing. *Virtual and Physical Prototyping*, **16**, 372-386. https://doi.org/10.1080/17452759.2021.1944229

[123] Zhu, Q., Liu, Z. and Yan, J. (2021) Machine Learning for Metal Additive Manufacturing: Predicting Temperature and Melt Pool Fluid Dynamics Using Physics-Informed Neural Networks. *Computational Mechanics*, **67**, 619-635. https://doi.org/10.1007/s00466-020-01952-9

[124] Matthes, S., Kluge, M., Jahn, S. and Emmelmann, C. (2020) Factors Influencing Powder-Properties of TiAl6V4 along the L-PBF Process Chain. *Progress in Additive Manufacturing*, **5**, 33-39. https://doi.org/10.1007/s40964-020-00120-y

[125] Shinkaryov, A.S., Cherkasova, M.V., Pelevin, I.A., Ozherelkov, D.Y., Chernyshikhin, S.V., Kharitonova, N.A., Gromov, A.A. and Nalivaiko, A.Y. (2021) Aluminum Powder Preparation for Additive Manufacturing Using Electrostatic Classification. *Coatings*, **11**, 629. https://doi.org/10.3390/coatings11060629

[126] Xiang, Z., Zhang, M., Yan, R., Yin, Q. and Zhang, K. (2021) Powder-Spreading Dynamics and Packing Quality Improvement for Laser Powder Bed Fusion Additive Manufacturing. *Powder Technology*, **389**, 278-291. https://doi.org/10.1016/j.powtec.2021.05.036

[127] Reverte, E., Calvo-Dahlborg, M., Dahlborg, U., Campos, M., Alvaredo, P., Martin-Rodriguez, P., Gordo, E. and Cornide, J. (2021) Design and Production of a New FeCoNiCrAlCu High-Entropy Alloy: Influence of Powder Production Method on Sintering. *Materials*, **14**, 4342. https://doi.org/10.3390/ma14154342

[128] Stemper, L., Tunes, M.A., Tosone, R., Uggowitzer, P.J. and Pogatscher, S. (2022) On the Potential of Aluminum Crossover Alloys. *Progress in Materials Science*, **124**, Article ID: 100873. https://doi.org/10.1016/j.pmatsci.2021.100873

[129] Svoboda, J., Boril, P., Holzer, J., Luptáková, N., Jary, M., Mašek, B. and Dymácek, P. (2022) Substantial Improvement of High Temperature Strength of New-Generation Nano-Oxide-Strengthened Alloys by Addition of Metallic Yttrium. *Materials*, **15**, 504. https://doi.org/10.3390/ma15020504

[130] Khrunyk, Y.Y., Ehnert, S., Grib, S.V., Illarionov, A.G., Stepanov, S. I., Popov, A.A., Ryzhkov, M.A., Belikov, S.V., Xu, Z., Rupp, F., *et al.* (2021) Synthesis and Characterization of a Novel Biocompatible Alloy, Ti-Nb-Zr-Ta-Sn. *International Journal of Molecular Sciences*, **22**, 10611. https://doi.org/10.3390/ijms221910611